AD_____

Award Number: DAMD17-01-1-0744

TITLE: Molecular Genetic Studies of Bone Mechanical Strain and of Pedigrees with Very High Bone Density

PRINCIPAL INVESTIGATOR: David J. Baylink, M.D.

CONTRACTING ORGANIZATION: Loma Lind Veterans Association for Research and Education
Loma Linda, California 92357

REPORT DATE: June 2003

TYPE OF REPORT: Annual

PREPARED FOR: U.S. Army Medical Research and Materiel Command
Fort Detrick, Maryland 21702-5012

REPORT DOCUMENTATION PAGE

Form Approved
OMB No. 074-0188

1. AGENCY USE ONLY (Leave blank)	2. REPORT DATE	3. REPORT TYPE AND DATES COVERED
	June 2003	Annual (15 May 2002 - 14 May 2003)

4. TITLE AND SUBTITLE
Molecular Genetic Studies of Bone Mechanical Strain and of Pedigrees with Very High Bone Density

5. FUNDING NUMBERS
DAMD17-01-1-0744

6. AUTHOR(S)
David J. Baylink, M.D.

7. PERFORMING ORGANIZATION NAME(S) AND ADDRESS(ES)
Loma Linda Veterans Association for Research and Education
Loma Linda, California 92357

E-Mail: baylid@lom.med.va.gov

8. PERFORMING ORGANIZATION REPORT NUMBER

9. SPONSORING / MONITORING AGENCY NAME(S) AND ADDRESS(ES)
U.S. Army Medical Research and Materiel Command
Fort Detrick, Maryland 21702-5012

10. SPONSORING / MONITORING AGENCY REPORT NUMBER

11. SUPPLEMENTARY NOTES

12a. DISTRIBUTION / AVAILABILITY STATEMENT
Approved for Public Release; Distribution Unlimited

12b. DISTRIBUTION CODE

13. ABSTRACT (Maximum 200 Words)

Our past studies have revealed that the bone formation response to physical activity is genetically regulated. During this grant period, we have devised the means to study the genes responsible for this genetic regulation in in-bred strains of mice. These genes are of utmost importance because of their potential effects on all living humans. These studies in mice will be complimented by *in vitro* studies that have provided exciting information on the signaling pathways involved in the variable bone formation response to exercise. This type of information is essential to a full understanding of this important adaptive process.

The second project is to perform genetic linkage analysis in a large pedigree with very high bone density, an analysis that could reveal genes important for providing diagnostic and treatment information. Phenotype and genotype data were collected and linkage analysis was performed by appropriate computer programs to locate two important loci for high bone density, chromosome 11 and chromosome 18. We are now engaged in fine mapping to identify the genes. The identity of the genes in these two loci could have important implications for our military with respect to susceptibility to battlefield injury and healing response to battlefield injury.

14. SUBJECT TERMS
OTL analyses; high bone density phenotype; microarray analyses; mechanical signaling; tyrosine phosphorylation; fluid flow shear strain; human genetic pedigree studies; linkage analyses;

15. NUMBER OF PAGES
61

16. PRICE CODE

17. SECURITY CLASSIFICATION OF REPORT	18. SECURITY CLASSIFICATION OF THIS PAGE	19. SECURITY CLASSIFICATION OF ABSTRACT	20. LIMITATION OF ABSTRACT
Unclassified	Unclassified	Unclassified	Unlimited

Table of Contents

I. Molecular Genetic Studies of Bone Mechanical Strain

1. Molecular Genetic Studies of Bone Mechanical Strain – in vivo studies

Introduction

Physical exercise is believed to increase bone formation and improve bone density in osteoporotic patients and other patients with metabolic disease as well as in novel subjects. However, the mechanisms by which mechanical stress converts mechanical signaling and activates a set of stress-responsible genes leading to bone remodeling are not fully understood. Our previous studies have shown that two inbred mouse strains, C57BL/6J (B6) and C3H/HeJ (C3H), respond differently to mechanical loading *in vivo*. B6 mice showed a significant increase in bone density as compared to C3H mice when subjected to similar loading regimens. These results suggest that mechanical stimulation may induce distinct types of gene expression in B6 mice, which contributes to the subsequent bone formation. Therefore, it is of particular interest to us to localize the chromosomal regions responsible to mechanical stress and identify osteogenic candidate genes by applying powerful genetic tools, namely quantitative trait loci (QTL).

Technical Objectives

Technical Objectives 1 and 2 for the past twelve months was revised on 04/15/03. The revised specific objectives for Technical Objective 1 are provided below. In the original proposal, there were two Technical Objectives for this portion of our work. The second Technical Objective has now been incorporated into the first Technical Objective. Therefore, on this progress report we will report on Technical Objective 1, and its five specific objectives. With the aforementioned revision, there is no longer a Technical Objective 2; Technical Objective 1 will then be followed by Technical Objective 3, which is a progress report on our *in vitro* work, to evaluate the physical actions of mechanical strain on bone cells *in vitro*.

Our specific objectives for the revised Technical Objective are:

1) To establish the optimal method for inducing mechanical strain on the tibia.
2) To determine the optimal method for quantitating the bone formation response to mechanical strain on the tibia *in vivo*.
3) To determine the number of days required of 4-point bending induced mechanical strain on the tibia in order to elicit an optimal response for quantitative measurements.
4) To select the optimal mouse inbred strain pair (i.e. B6 and C3H or some other strain pair) to perform the QTL mapping study.
5) To determine the appropriate age of animals to apply the 4-point bending in order to obtain valid quantitative measurements of the bone formation response.

Our goal is to evaluate the bone formation in 10 different mouse strains using mechanical loading in order to identify two mouse strains which show extreme differences in the bone formation. These selected strains will then be backcrossed for two more generations (F2) and the F2 mice will be used to identify candidate genes responsible for bone formation by applying a powerful genetic tool, quantitative trait loci (QTL), as described previously. Initially we had planned to perform the jump training as a loading model. However, if jump training does not show a significant amount of bone formation, then we will be using four-point bending as alternative loading regimen and real time PCR as the end point measurement of the bone formation rate in two strains that show extreme difference in bone formation.

This report includes our progress for the last twelve months of our proposal (May 2002-May 2003).

Specific Objective 1: Optimize a method that can induce mechanical strain on bone.

Initially, 6-week old B6 mice were given 4-days jump-up and jump-down training to evaluate the bone formation response. The mice were sacrificed after 24hrs of the last training regimen and the bone formation was evaluated in terms of mRNA expression using Real time PCR. In this experiment, we used type-I collagen since it constitutes approximately 95% of bone matrix and will therefore show increased expression in response to loading. However, we found that the jump training did not produce a sufficient amount of stress on the bone to see a significant change in the expression of type-I collagen between control and experiment (Table-1). The values in the table represent the cycles (Ct-values), which correspond to the amount of amplified product of the target gene.

Table-1 Quantification of type-1 collagen expression in 6-week old B6 mice in response to jump training using real time PCR. The value represents Mean ± SD.

Experiments	Groups	Cycles ± SD		
		Gene	0.1μg of RNA	Fold Change
JUMP DOWN-20cm				
	Control	Col A1	19.56 ± 1.03	No change
	Jump-down 20 cm	Col A1	24.40 ± 0.97	No change
	Control	β-actin	23.49 ± 1.07	No change
	20cm Jump-down	β-actin	22.69 ± 0.96	No change
JUMP-DOWN-40cm				
	Control	Col A1	19.83 ± 0.72	No change
	Jump-down 40cm	Col A1	19.40 ± 0.7	No change
	Control	β-actin	21.98 ± 0.51	No change
	40cm Jump-down	β-actin	22.75 ± 1.12	No change
JUMP-UP 20cm				
	Control	Col A1	28.32 ± 2.06	No change
	Jump-up 20cm	Col A1	28.65 ± 1.22	No change
	Control	β-actin	34.72 ± 2.56	No change
	Jump-up 20cm	β-actin	35.51 ± 1.33	No change

N=4, p>.05 for all co-variance
ColA1-type-1 collagen, β-actin-beta-actin

Therefore, we used our next candidate *in-vivo*-loading regimen, namely four-point bending. The load, cycle, and frequency used for the study were similar to that used by Reckers, et al., (1998), except the duration of training was changed from 12 to 4-days of training in order to evaluate the effect of mechanical strain on bone formation in a short duration. The loading regimen consists of a 9N load at 2Hz for 36cycles. The training is preformed once per day. The right tibia of the mouse is loaded while the left tibia is used as an internal control. The mice are sacrificed 24 hrs after the last training regimen and the mRNA message is quantified using Real time PCR. In this experiment, in order to evaluate the bone formation in response to loading, we used two major bone markers, namely type-I collagen and osteocalcin. In addition to this, we also used other bone formation genes namely bone sialoprotein, alkaline phosphate, osteocalcin and osteopontin.

Four days four-point bending in 16-week old B6 and C3H mice showed a significant ($p<0.05$) increase in the expression of bone formation genes in loaded bones as compared to unloaded bones. As shown in Table-2&3, mechanical loading resulted in two-fold increase in

type-I collagen, bone sialoprotein, and alkaline phosphates in both B6 and C3H mice. However, B6 mice showed 1.4-fold increase in Osteocalcin while C3H did not show any change between unloaded and loaded bones.

Table-2 Quantitative Real time PCR results in response to 4-days training of four-point bending in 16-week old B6 mice using 200 ng RNA concentration.

Genes	Groups	Cycles ± SD	P-value	Fold Change
Type-I Collagen	Experiment	20.17 ± 1.37	0.02 [a]	2.2
	Control	18.45 ± 0.49		
Osteocalcin	Control	24.60 ± 0.86	0.05 [a]	1.42
	Experiment	23.49 ± 0.70		
Bone sialoprotein	Control	25.11 ± 0.97	0.01 [a]	2.2
	Experiment	23.20 ± 0.59		
Alkaline Phosphatase	Control	29.53 ± 1.34	0.02 [a]	2.5
	Experiment	27.60 ± 0.64		
Osteopontin	Control	24.01 ± 1.38	0.38	No change
	Experiment	23.36 ± 0.77		
	Control	19.19 ± 1.04		
Actin	Experiment	18.60 ± 0.49	0.28	

N = 5,, [a]p<0.05

Table-3 Quantitative Real time PCR results in response to 4-days training of four-point bending in 16-week old C3H mice using 200 ng RNA concentration.

Genes	Groups	Cycles ± SD	P-value	Fold Change
Type-I collagen	Control	23.77 ± 1.05	0.0002*	3.0
	Experiment	20.47 ± 0.58		
Osteocalcin	Control	26.16 ± 0.86	0.10	No change
	Experiment	25.30 ± 0.76		
Bone sialoprotein	Control	27.06 ± 1.85	0.02 [a]	1.52
	Experiment	24.74 ± 0.57		
Alkaline Phosphatase	Control	31.10 ± 1.31	0.003*	2.0
	Experiment	28.37 ± 0.65		
Bone Osteopontin	Control	26.92 ± 1.62	0.25	No change
	Experiment	25.89 ± 0.93		
	Control	22.82 ± 1.68	0.07	
Actin	Experiment	21.11 ± 0.84		

*N= 4, [a]p<0.05, *p<0.01*

Specific Objective 2: Determine an optimal method to evaluate the bone formation

To quantify the peak gene expression in response to loading, we used a technique called real time PCR. After the training regimen, mice are sacrificed and the total RNA is extracted from the loaded and unloaded bone by Trizol method. This RNA is used to synthesis single strand cDNA by reverse transcription assay followed by Real time PCR using applied biosystems. The principle of this Real time PCR is similar to an ordinary PCR except with a fluorescent dye which binds to amplified product and emits fluorescence signals that are viewed in terms of cycles or

Ct-values. The Ct-values correspond to the amount of amplified products and used for calculating the mRNA expression of the target gene. In order to validate these Ct-values, we also run Universal RNA (Stratagene, USA) as a standard during each reaction. We used SYBR Master mix (Fluorescent PCR reagents) kit to perform the above reaction in applied biosystems. In this four-point bending experiment, to evaluate the bone formation response to loading we used two major bone markers, namely type-I collagen and osteocalcin. In addition to this, we also used other bone formation genes, namely bone sialoprotein, alkaline phosphatase, and osteopontin, since they play a significant role in the mineralization of bone. B-actin was used as an internal control to normalize the data and calculate the exact fold change of genes by applying a mathematical formula ($2^{-\Delta\Delta CT}$) of applied biosystems.

In order to further validate the four-point bending method and the real time PCR results, we used pQCT and histological methods that are well-established endpoints for measuring the bone formation. We performed 12-days training of four-point bending with similar magnitude of load, frequency and cycle number in 16-week B6 and C3H mice. Since longer periods of time are required to see new bone deposit, we used 12 days of training instead of 4 days. As shown in Fig.1, 12-days training in 16-week B6 mice showed maximum change in total area, total content, and cortical content in the loaded bones compared to unloaded bones. Significant changes were also observed in periosteal, endosteal circumference, and bone density.

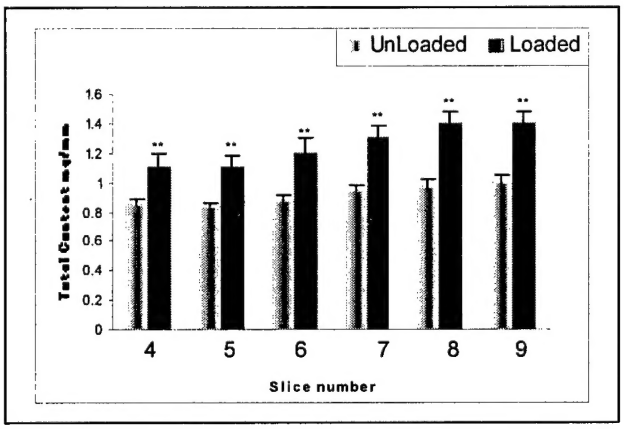

Fig.1 [a]

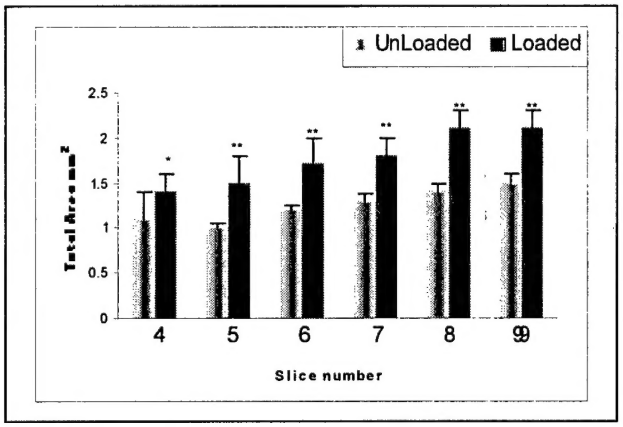

Fig.1 [b]

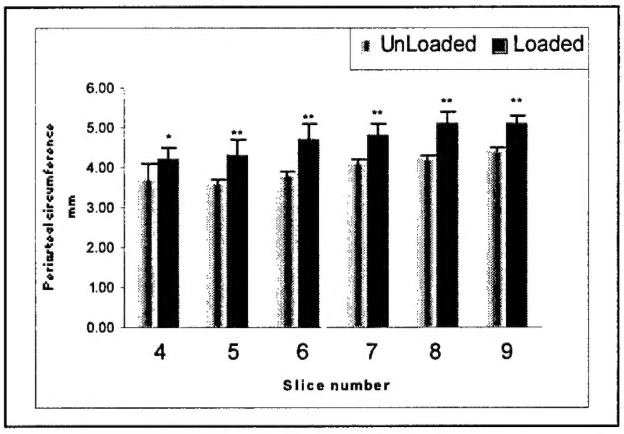

Fig.1 [c]

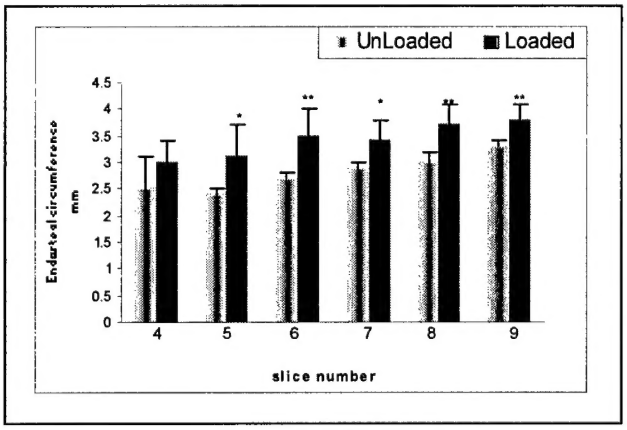

Fig.1 [d]

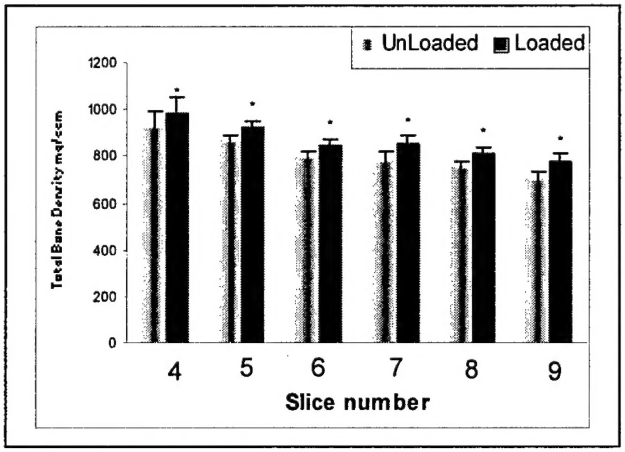

Fig.1 [e]

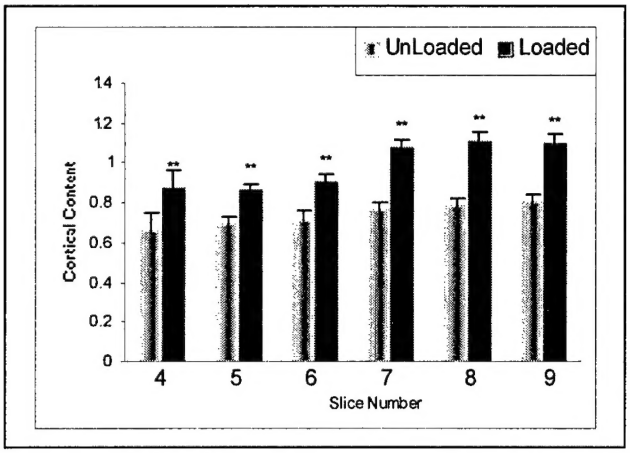

Fig.1 [f]

Fig.1 Changes in bone formation parameters in response to 12 days training of four-point bending measured by pQCT in tibia of 16-week female B6 mice. The data for slice 4-9 which represents loading zone are shown as mean $\pm$ standard deviation (n=9). P-values are calculated using t-test comparing the loaded and unloaded bones.

(a) Total content shows $p<0.001^{**}$
(b) Total area shows $p<0.001^{**}$ for all the slices except slice-4 with $p<0.01^{*}$
(c) Periosteal circumference shows $p<0.001$ for all the slices except for slice-4 with $p<0.01^{*}$
(d) Endosteal circumference shows $p<0.001^{**}$ for slice 6,8,9 and for slice 5, 7 $p<0.01^{*}$ while slice 4 $p>0.05$
(e) Cortical content shows $p<0.001^{**}$ for all the slices
(f) Total Density showed $p<0.01^{*}$ for all the slices

Similar to the B6, C3H mice also showed maximum change in total area, total content, periosteal and endosteal circumference of bone in response loading. However, in contrast to the B6, there was no change in total density in the loaded bones compared to unloaded bone as shown in Fig.2.

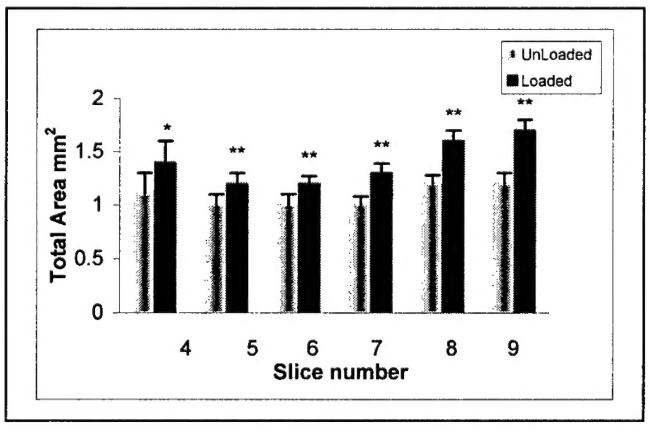

Fig.2 [a]

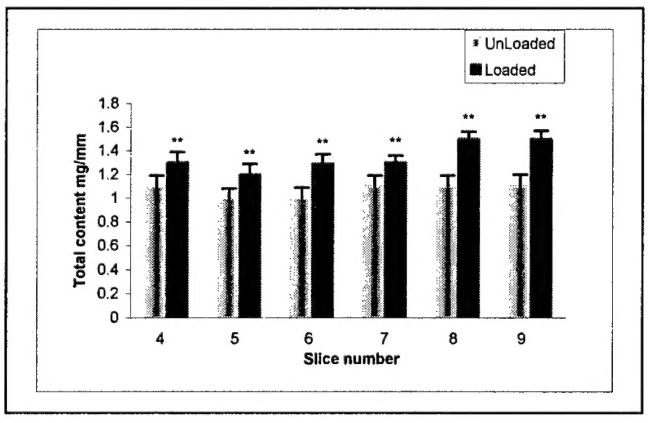

Fig.2 [b]

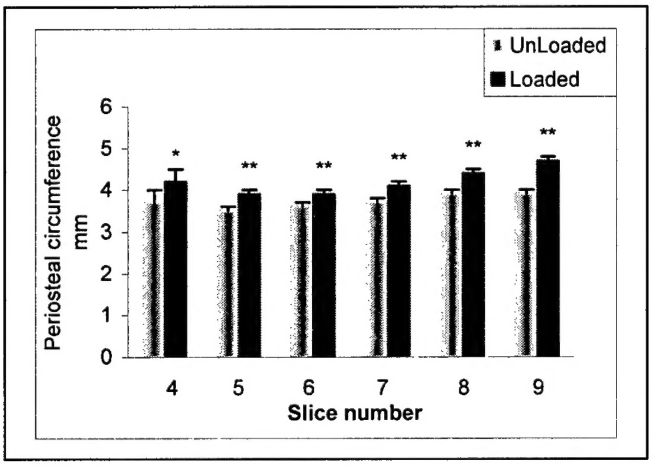

Fig.2 [c]

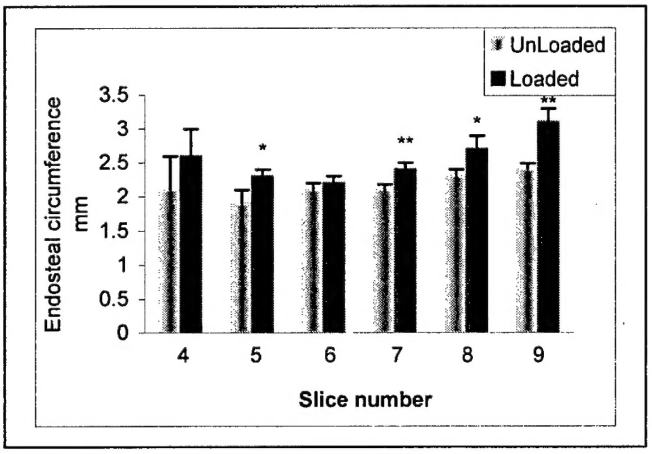

Fig. 2 [d]

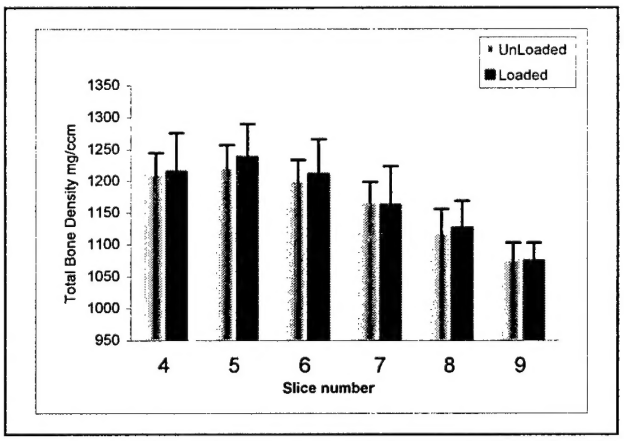

Fig.2 [e]

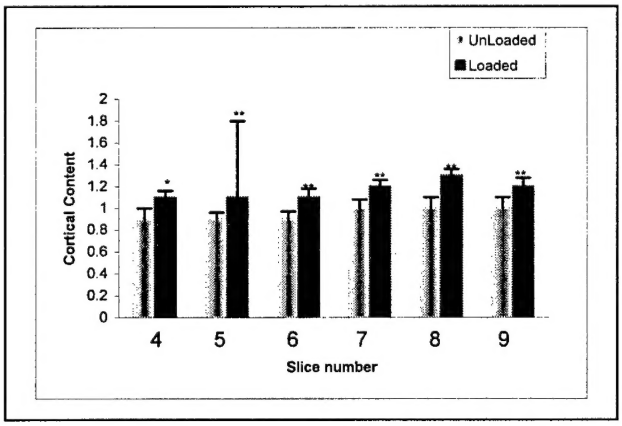

Fig.2 [f]

Fig.2 Changes in bone formation parameters in response to 12 days of four-point bending measured by pQCT in tibia of 16-week female C3H mice. The data for slice 4-9 which represents mean $\pm$ standard deviation (n=9). P-values are calculated using t-test comparing the loaded and unloaded bones.

a) Total Content shows $p < 0.001^{**}$
b) Total area show $p<0.001^{**}$ for all the slices except for slice-4 $p<0.05^{a}$
c) Periosteal circumference shows $p<0.001^{**}$ except for slice-4 $p<0.01^{*}$
d) Endosteal circumference shows $p<0.001^{**}$ for slices 7, 9 while slices 5, 8 showed $p<0.01^{*}$. Slices 4 &6 showed $p>0.05$
e) Total bone density shows $p>0.05$ for all the slices
f) Cortical Content shows $p<0.001^{**}$ for all the slices except slice-4 with $p<0.01^{*}$

Furthermore, to correlate the pQCT and gene expression results using real time PCR in response to mechanical loading, we performed 12 days of four-point bending in retired breeders of B6 and C3H mice. Twelve days training of four-point bending in B6 retired breeders showed 9-fold increase in type-I collagen (ColA1) and 7-fold increase in alkaline phosphatase (ALP) as compared to C3H retired breeders. However, the bone sialoprotein showed a decrease in fold change for B6 compared to C3H. This suggests that long durations of bending treatment

decreased the expression of bone sialoprotein in B6 (Fig.3). Based on these results, type-I collagen found to be a valuable marker that is increased in all age groups in response to bending. On the other hand, 12 days of four-point bending using pQCT showed increase in total area, total content, periosteal, and endosteal circumference of bone for B6 mice compared to C3H mice of retired breeders as shown in Fig.3a. However, for the total density, B6 showed very less change while C3H showed no significant change.

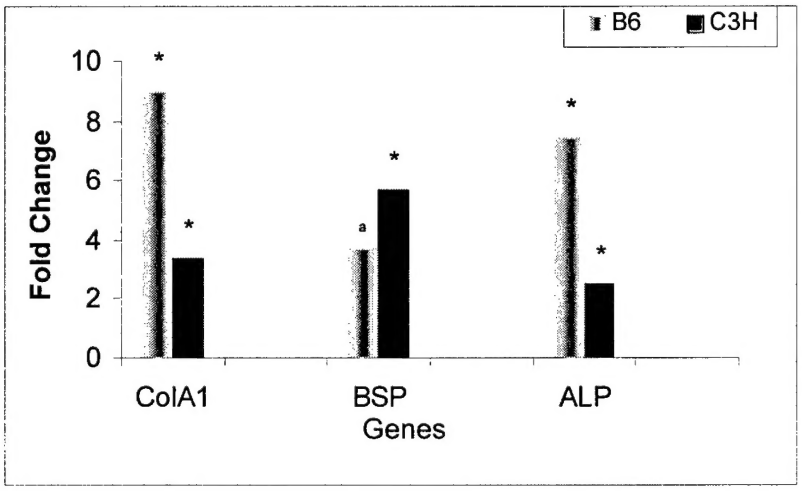

N=5, * *$p<0.01$,* $^{a}p<0.05$*

Fig.3 Fold change in expression of various genes in response to 12 days of four-point bending in B6 and C3H retired breeders.

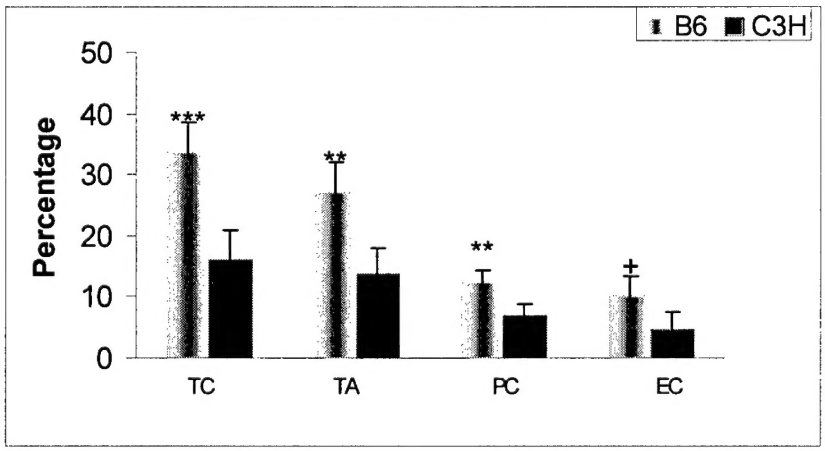

$^{***}p<0.0001$, $^{**}p<0.001$, $^{+}p<0.05$

Fig.3a Increase in bone formation parameters in response to 12 days training of four-point bending measured by pQCT in tibia of B6 and C3H retired breeders. The data shows percentage of increase in TA-Total Content, TA-Total Area, PC-Periosteal circumference, EC-Endosteal circumference as Mean $\pm$ Standard deviation of loaded zone. P-values are calculated by comparing the percentage of new bone formation between B6 and C3H mice.

We used Real-time PCR and pQCT as two methods for measuring the bone formation rate in response to four-point bending. Fig.3b shows the correlation between Bone Mineral

Density and Type-I Collagen expression. As shown, there is a significant correlation ($p<0.05$) between the BMD [Measured by pQCT] and collagen expression [Measured by real time PCR]. Based on these results, we conclude that Real time PCR is the most sensitive and fastest method to evaluate the bone formation in response to four-point bending. Thus, we will be using Real Time PCR as the endpoint in our QTL study.

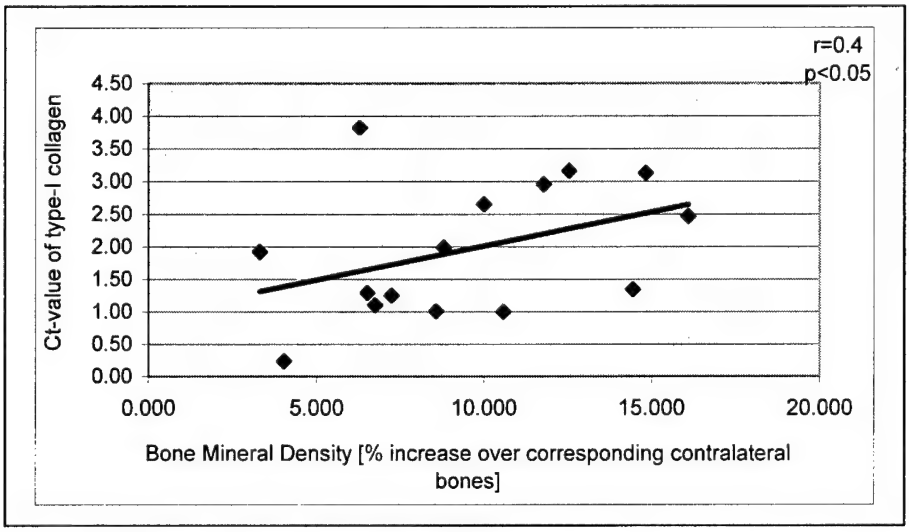

Fig.3b Correlation between bone mineral density and type-I collagen expression in response to four-point bending in different age groups of B6 mice. The x-axis represents BMD change measured by percentage increase in loaded bone compared to corresponding contralateral bone. The y-axis shows change in collagen gene expression in response to four-point bending as measured by $^{\Delta\Delta}$Ct for loaded bone vs unloaded bone using b-actin as control gene.

Specific Objective 3: Determine an optimal duration of Training period

Ten-week old B6 mice were subjected to 2 days, 4 days and 8 days training in order to select an optimal duration of training that show maximum effect on bone formation. 2 days of four-point bending in B6 mice did not produce any significant effect on bone. The expression of bone formation genes in loaded bones was similar to the control shown in Table-4.

Table -4 Quantitative Real time PCR results in response to 2 days training of four-point bending in 10-week old B6 mice using 200 ng RNA concentration.

Genes	Groups	Cycles ± SD	P-value	Fold Change
Type-I collagen	Control	20.61 ± 1.9	0.97	
	Experiment	20.58 ± 0.4		No change
Osteocalcin	Control	24.85 ± 2.2	0.52	
	Experiment	24.17 ± 0.6		No change
Bone sialoprotein	Control	26.59 ± 1.4	0.82	
	Experiment	26.76 ± 0.59		No change
Alkaline Phosphatase	Control	30.70 ± 1.9	0.86	
	Experiment	30.86 ± 0.5		No change
	Control	22.40 ± 2.4	0.48	Internal control
Actin	Experiment	21.60 ± 0.49		

N=5, p>0.05

Four days four-point bending in 10-week old B6 mice resulted in 2.9 and 4.5 fold increase in type-1- collagen and bone sialoprotein respectively. On the other hand, no change was observed in alkaline phosphates, osteocalcin and osteopontin (Table-5). B-actin was used as internal control to normalize the data in order to obtain the fold change of the target gene.

Table-5 Quantitative Real time PCR results in response to 4 days four-point bending in 10-week old B6 mice using 200 ng RNA concentration.

Genes	Groups	Cycles ± SD	P-value	Fold Change
Type-I Collagen	Experiment	21.75 ± 1.8		
	Control	19.45 ± 1.5	0.06	2.9
Bone sialoprotein	Control	27.21 ± 1.4		
	Experiment	24.22 ± 1.9	0.02[a]	4.5
Osteocalcin	Control	25.28 ± 1.1		
	Experiment	24.76 ± 1.06	0.49	No change
Alkaline phosphatase	Control	31.88 ± 2.4		
	Experiment	29.55 ± 2.1	0.14	No change
Osteopontin	Control	24.36 ± 1.3		
	Experiment	23.57 ± 1.1	0.34	No change
	Control	22.56 ± 1.6		
Actin	Experiment	21.84 ± 1.3	0.47	Internal Control

N=5, [a] *$p<0.05$*

Eight days of four-point bending in tibia of 10-week old B6 mice showed significant change in expression of bone formation genes compared to 2-days and 4-days of training. As shown in Table-6, 8-days of training showed 4-fold increase in type-I collagen, 2.7-fold in osteocalcin, 3.6 fold in Bone sialoprotein and 2.8 fold in alkaline phosphotase.

Table-6 Quantitative Real time PCR results in response to 8 days four-point bending in 10-week old B6 mice using 200 ng RNA concentration.

Genes	Groups	Cycles ± SD	P-value	Fold Change
Type-I collagen	Control	22.02 ± 0.4	0.00001**	3.8
	Experiment	19.35 ± 0.4		
Osteocalcin	Control	24.94 ± 1.1	0.01[a]	2.7
	Experiment	22.76 ± 0.9		
Bone sialoprotein	Control	26.79 ± 0.8	0.003*	3.7
	Experiment	24.16 ± 1.1		
Alkaline Phosphatase	Control	29.78 ± 0.9	0.001*	2.9
	Experiment	27.53 ± 0.5		
	Control	22.56 ± 1.1	0.24	Internal control
Actin	Experiment	21.83 ± 0.6		

N=5, * *$p<0.01$,* ** *$p<0.001$,* [a] *$p<0.05$*

Specific Objective 4: Determine optimal mouse strain pair that show extreme difference in bone formation.

With the optimized loading regimen, four-point bending was carried out in 10-week-old B6, Balbc, AKR/J, 129J, NZB mice and the bone formation was evaluated using Real time PCR. AKR/J showed one-fold change in type-I collagen, alkaline phosphatase, and two-fold change in Bone sialoprotein while no change in osteocalcin was seen (Table-7). 129J showed 3 fold change in type-I collagen and bone sialoprotein. However, no change in alkaline phosphatase, osteocalcin, and osteopontin was observed (Table-8). NZB showed no change in any of the bone markers in response to four-point bending (Table-9). In the case of Balbc, the bone (tibia) broke at 9N load, therefore, a 6N load was applied. There was no change in expression of bone formation genes between control and experiment in Balbc mice (Table-10). The B6 mice showed three-four fold increase in type-I collagen and bone sialoprotein. However, there was no change in alkaline phosphatase and osteocalcin (Table-11). Overall, AKR, 129J and B6 mice showed similar gene expression in response to four-point bending while Balbc and NZB showed no significant change in expression of bone formation genes shown in Table-12

Table-7 Quantitative Real time PCR results in response to 4-days four-point bending in 10-week old AKR/J using 200 ng RNA concentration.

Genes	Groups	Cycles ± SD	P-value	Fold Change
Type-I Collagen	Experiment	18.16 ± 0.9	0.01 [a]	1.0
	Control	19.35 ± 0.4		
Bone sialoprotein	Control	25.27 ± 1.7	0.01 [a]	2.7
	Experiment	22.76 ± 1.1		
Alkaline Phosphatase	Control	24.23 ± 0.8	0.02 [a]	1.3
	Experiment	22.87 ± 0.9		
Osteocalcin	Control	22.11 ± 0.4	0.44	No change
	Experiment	21.74 ± 1.0		
	Control	20.73 ± 1.5	0.1	Internal control
Actin	Experiment	19.65 ± 0.9		

N=5, [a]p<0.05

Table-8 Quantitative Real time PCR results in response to 4-days four-point bending in 10-week old 129J using 200 ng RNA concentration.

Genes	Groups	Cycles ± SD	P-value	Fold Change
Type-I Collagen	Experiment	20.87 ± 0.7	0.06	2.6
	Control	19.66 ± 0.9		
Bone sialoprotein	Control	23.48 ± 0.3	0.05 [a]	2.8
	Experiment	22.14 ± 1.3		
Alkaline Phosphatase	Control	27.33 ± 1.3	0.57	No change
	Experiment	26.80 ± 1.5		
Osteopontin	Control	29.33 ± 0.4	0.37	No change
	Experiment	29.93 ± 1.3		
Osteocalcin	Control	26.49 ± 0.6	0.53	No change
	Experiment	26.26 ± 0.4		
	Control	19.62 ± 1.1	0.53	Internal Control
Actin	Experiment	20.07 ± 1.0		

N=5, [a] *$p<0.05$*

Table-9 Quantitative Real time PCR results in response to 4-days four-point bending in 10-week old NZB using 200 ng RNA concentration.

Genes	Groups	Cycles ± SD	P-value	Fold Change
Type-I Collagen	Experiment	19.50 ± 2.4	0.63	No change
	Control	18.94 ± 1.3		
Bone sialoprotein	Control	23.89 ± 1.6	0.12	No change
	Experiment	24.77 ± 2.6		
Osteocalcin	Control	22.16 ± 1.7	0.50	No change
	Experiment	24.13 ± 2.3		
	Control	20.86 ± 1.4	0.31	Internal control
Actin	Experiment	21.92 ± 1.9		

N=5, $p>0.05$

Table-10 Quantitative Real time PCR results in response to 4-days four-point bending in Balbc10-week old mice using 200 ng RNA concentration.

Genes	Groups	Cycles ± SD	P-value	Fold change
Type-I Collagen	Experiment	17.80 ± 1.4	0.98	No change
	Control	17.78 ± 1.7		
Bone sialoprotein	Control	23.32 ± 1.5	0.49	No change
	Experiment	22.59 ± 1.5		
Alkaline Phosphatase	Control	25.32 ± 2.1	0.81	No change
	Experiment	25.00 ± 1.4		
Osteopontin	Control	28.51 ± 2.0	0.88	No change
	Experiment	28.35 ± 1.1		
	Control	17.86 ± 1.0	0.33	Internal control
Actin	Experiment	17.21 ± 0.9		

N=5 p>0.05

Table-11 Quantitative Real time PCR results in response to 4 days training of four-point bending in 10-week old B6 mice using 200ng RNA concentration

Genes	Groups	Cycles ± SD	P-value	Fold Change
Type-I Collagen	Experiment	21.75 ± 1.8	0.06	2.9
	Control	19.45 ± 1.5		
Bone sialoprotein	Control	27.21 ± 1.4	0.02 [a]	4.5
	Experiment	24.22 ± 1.9		
Osteocalcin	Control	25.28 ± 1.1	0.49	No change
	Experiment	24.76 ± 1.0		
Alkaline phosphatase	Control	31.88 ± 2.4	0.14	No change
	Experiment	29.55 ± 2.1		
Osteopontin	Control	24.36 ± 1.3	0.34	No change
	Experiment	23.57 ± 1.1		
Actin	Control	22.56 ± 1.6	0.47	Internal control
	Experiment	21.84 ± 1.3		

N=5, [a]p-<0.05

Table-12 Ranking of mouse strain [Good and Poor responder] based upon the expression of bone formation genes in response to 4 days of four-point bending.

Bone Formation Markers	Fold change in response to 4-days training of four-point bending in different inbred strains of mice [10-week old]				
	Good Responder			**Poor Responder**	
Genes	B6	**129J**	**AKR/J**	**NZB**	**Balbc**
Type-I collagen	2.9	2.6	1.0	-	-
Bone sialoprotein	4.5	2.8	2.7	-	-
Alkaline phosphatase	-	-	1.3	-	-
Osteocalsin	-	-	-	-	-

- No change

Specific Objective 5: Determine appropriate age of mice that shows significant affect on bone formation through optimized protocol.

With the optimized loading regimen [9N load at 2Hz –36cycles] four-point bending was applied B6 mice of 10-week old, 16-week old and Retired Breeders and the bone formation was evaluated using real time PCR. As shown in Table-13, 10-week old mice in response to 4-days

training showed increased expression of type-I collagen and Bone sialoprotein (p-<0.05) while no change in osteocalcin and alkaline phosphates. While 16-week old mice showed two-fold change in type-I collagen, bone sialoprotein, alkaline phosphates and 1.4 fold change in osteocalcin shown in Table-14. Interestingly in the retired breeders we found that increase in age show a better response of bone formation in response to 4-days training of 9N load. The type-I collagen and Bone sialoprotein showed a significant fold change with p<0.01 while alkaline phosphotase and osteocalcin showed p<0.05 (Table-15).

Table-13 Quantitative Real time PCR results in response to 4-days four-point bending in 10-week old female B6 mice using 200 ng RNA concentration

Genes	Groups	Cycles ± SD	P-value	Fold Change
Type-I Collagen	Experiment	21.75 ± 1.8	0.06	2.9
	Control	19.45 ± 1.5		
Bone sialoprotein	Control	27.21 ± 1.4	0.02 [a]	4.5
	Experiment	24.22 ± 1.9		
Osteocalcin	Control	25.28 ± 1.1	0.49	No change
	Experiment	24.76 ± 1.06		
Alkaline phosphatase	Control	31.88 ± 2.4	0.14	No change
	Experiment	29.55 ± 2.1		
Osteopontin	Control	24.36 ± 1.3	0.34	No change
	Experiment	23.57 ± 1.1		
Actin	Control	22.56 ± 1.6	0.47	Internal control
	Experiment	21.84 ± 1.3		

N=5, [a]p<0.05

Table-14 Quantitative Real time PCR results in response to 4-days four-point bending in 16-week old female B6 mice using 200 ng RNA concentration.

Genes	Groups	Cycles ± SD	P-value	Fold Change
Type-I Collagen	Experiment	20.17 ± 1.37	0.02 [a]	2.2
	Control	18.45 ± 0.49		
Osteocalcin	Control	24.60 ± 0.86	0.05 [a]	1.42
	Experiment	23.49 ± 0.70		
Bone sialoprotein	Control	25.11 ± 0.97	0.01 [a]	2.2
	Experiment	23.20 ± 0.59		
Alkaline Phosphatase	Control	29.53 ± 1.34	0.02 [a]	2.5
	Experiment	27.60 ± 0.64		
Osteopontin	Control	24.01 ± 1.38	0.38	No change
	Experiment	23.36 ± 0.77		
Actin	Control	19.19 ± 1.04	0.28	Internal control
	Experiment	18.60 ± 0.49		

N = 5, [a]p<0.5

Table-15 Quantitative Real time PCR results in response to 4 days four-point bending in B6 Retired breeders using 200 ng RNA concentration

Genes	Groups	Cycles ± SD	P-value	Fold Change
Type-I collagen	Control	22.26 ± 1.0	0.0007*	6.5
	Experiment	18.61 ± 0.54		
Bone sialoprotein	Control	25.58 ± 1.1	0.002*	6.5
	Experiment	21.93 ± 0.98		
Alkaline phosphotase	Control	30.16 ± 1.5		
	Experiment	27.14 ± 1.2	0.02 [a]	4
	Control	27.28 ± 1.0		
Osteocalcin	Experiment	25.33 ± 1.1	0.04 [a]	2
	Control	20.82 ± 0.64	0.12	Internal control
Actin	Experiment	19.88 ± 0.82		

N = 4, [a]p-<0.05, *p-<0.01

Key Findings

1. Determination of an appropriate response parameter. Because pQCT is a time-consuming labor-intensive method, we sought a more rapid, but yet sufficiently sensitive, method for measuring bone formation and response to mechanical loading. Measurement of bone marker expression by real time PCR has not been previously used to evaluate bone formation in a quantitative manner. Therefore, it was important for us to correlate the changes within an acceptable bone formation measurement, namely pQCT with our data obtained from real time PCR on gene expression. In this study, we found a good correlation between the real time PCR changes and the pQCT changes (pQCT is a measure of bone density whereas we have interpreted this to indicate bone formation simply because the amount of change in bone density is a reflection of bone formation). In conclusion, we found that real time PCR evaluating specific bone marker genes fulfilled our criteria for a sensitive reproducible and producible measurement that shows a nice response to four-point bending.

2. Duration of application of mechanical strain. Our studies indicate that four days of four-point bending in our femoral *in vivo* loading regimen is adequate for a measurable response in our proposed QTL studies.

3. Identification of bone response. These are genes that can be assayed as a group in real time PCR for assessment of the bone formation response to four-point bending. We found that alkaline phosphatase, osteocalsin, bone sialoprotein, and type-1 collagen genes showed statistically significant increases in RNA harvested from bone tissue following four days of four-point bending. Consequently, these genes were selected for further application.

4. Determination of the animal chronological age for application of four-point bending. We found that retired breeder mice and 16-week old mice showed the greatest increase in our bone formation parameters in response to four-point bending. However, we would prefer to use mice 10 weeks of age since we could progress in our QTL studies much more rapidly by using the younger mice. We are now in the process of settling whether we can use the 10-week old mice for our four-point bending QTL study.

5. The two strains of mice most appropriate for the four-point bending QTL study. In addition to C3 and B6 animals we have studied four additional strains; AKR, 129J, NZB, and the Balb/c mice. The AKR and the 129J showed a good response whereas the NZB and the Balb/c showed no response. We are now in the process in determining whether some combination of these latter four strains would be superior to the C3 and B6 for the high and low response pair.

Reportable Outcomes

None

Conclusions

1. Goals to accomplish before beginning the QTL studies. We have now completed all of the goals required for QTL studies except one, which we did not, include in our technical objective namely a dose response. Apart from that, we are ready to begin the QTL study. We are now in the process of doing a dose response to determine the optimal response range which best distinguishes the two different strains of mice, the C3H mice and B6 mice.

2. Selection of the optimal strains of mice. Based on the data so far, the C3H and B6 mice are the best strain pair and as mentioned above the final decision on this issue will be based on the dose response.

3. Real time PCR measurements of bone markers as a surrogate for pQCT measurement. When we plotted type-I collagen as our real time PCR measurement and the increment in pQCT bone density over the unloaded bone control bone, we found a significant correlation, which supports the view that we can use real time PCR as a much faster means to obtain our phenotype after four-point bending.

4. Additional phenotypes. Not only can we use these measurements of message level of bone proteins as indices of the bone formation response, we can also use them separately to evaluate their level of expression as a separate phenotypes to determine the QTLs responsible for quantitative level of expression of each real time PCR mRNAs.

References

1) Akhter MP, Cullen DM, Pedersen EA, Kimmel DB, Recker RR. Bone response to *in vivo* mechanical loading in two inbreeds of mice. Calcif Tissue Int 1998 Nov; 63(5):442-9.
2) Kodama Y, Uemura Y, Nagasawa S, Beamer WG, Donahue LR, Rosen CR, Baylink DJ, Farley JR. Exercise and mechanical laoding increase periosteal bone formation and whole bone strength in C57BL/6J mie but not in C3H/Hej mice. Calcif Tissure Int 2000 Apr; 66(4):298-306.

2. Molecular Genetic Studies on Bone Mechanical Strain – in vitro studies

Introduction

It is well established that mechanical loading leads to an increase in bone density and that immobilization leads to a loss in bone density. Although the response of bone cells to mechanical stimuli is relatively well understood, the knowledge about the signaling mechanisms and the genes involved in the mechanical regulation of bone structure and function are less understood or limited. In our recent study we have shown that two inbred strains of mice (C3H and B6) showed differing responses in bone turnover to mechanical loading, suggesting that the genetic component of bone response to mechanical loading must be biologically significant. To identify the genetic component involved, our goal is to apply a powerful genetic approach known as quantitative trait loci (QTL) in combination with *in vitro* studies on the biochemical pathways involved in mechanical stress signaling in order to determine the genes responsible for the mechanical stress differential responses between the two inbred strains of mice that show good and poor response of bone formation.

Technical Objectives:

To evaluate the effects of mechanical signaling using a physiologically relevant CytoDyne flow chamber to produce a fluid flow shear strain for evaluation of proliferation and differentiation and also for studies of gene expression and signal transduction pathways in cultures of C3H and B6 mouse osteoblasts. We will have the following specific objectives during the second year of this grant period:

1) We will complete our initial evaluation of strain-induced tyrosine phosphorylation levels of key signaling proteins by immunoprecipitation-immunoblotting approach using available antibodies. This technology will be applied to compare the responses of C3H vs. B6 mice.
2) Apply in-house microarrays to evaluate changes in gene expression of those genes known to be involved in mediating loading signal.
3) The genes that we identified by the above technique (i.e., the microarray technique) will be further compared with real time PCR.

In our previous report, we optimized the conditions to develop an *in vitro* system to apply defined mechanical strain to cultured bone cells and compared the phenotypic differences between the C3H and B6 mice in response to fluid flow shear stress. We found that osteoblasts isolated from B6 mice were highly responsive to shear stress in terms of cell proliferation and differentiation. On the other hand, osteoblasts isolated from C3H mice were unresponsive to the same shear stress. The following is our progress toward each of our objectives during Year 2 of this period (i.e., the last 12 months).

Specific Objective 1: Evaluate strain-induced tyrosine phosphorylation levels of key signaling proteins in C3H and B6 mice.

In order to clarify the signaling pathways which could lead to the changes in the fluid flow induced cell proliferation and differentiation in B6 bone cells and not in the bone cells isolated from C3H mice, we studied the fluid flow induced phosphorylation of MAPK and integrin expression in these cells, since the MAPK pathway and the integrin pathway have each been implicated in the mechanical signaling mechanism. As shown in Figure 1, fluid flow did not have any significant effect on the integrin β1expression in the C3H bone cells. Interestingly, B6 bone cells showed a significant increase in the integrin β1 expression when subjected to fluid flow. These findings suggest that shear stress- induced osteoblast proliferation and differentiation

in B6 mice may be associated with the shear stress-dependent upregulation of integrin β1 expression.

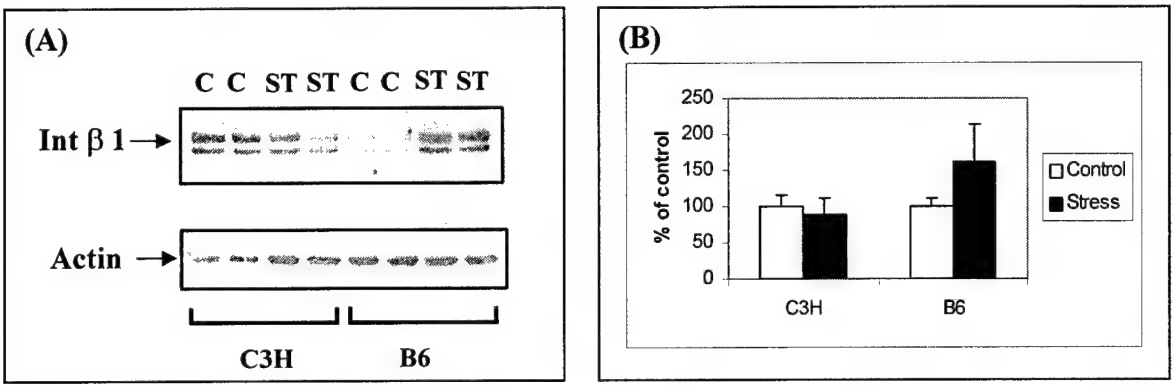

Figure 1. Effect of shear stress on integrin β1 in osteoblasts isolated from C3H and B6 mice. Cells were subjected to fluid flow of 20 dynes/cm2 for 30 minutes. **(A).** Cell lysates were immunoblotted with anti-integrin β1 and anti-actin antibodies. **(B).** The graph represents the densitometric measurements of integrin β1 levels from western blots normalized by actin.

Further, when the effect of fluid flow on MAPK phosphorylation was studied, it was observed that there was a significant increase in the phosphorylation levels of both the ERK1 and ERK2 in B6 bone cells when subjected to fluid flow. However, in C3H bone cells, no change was noted either in ERK1 or ERK2 phosphorylation levels in response to fluid flow (Figure 2). These findings suggest that the ERK signaling pathway is essential in the osteogenic response to mechanical stimuli in B6 bone cells. However, a remaining key question is whether activation of either ERK1 or ERK2 or both is required.

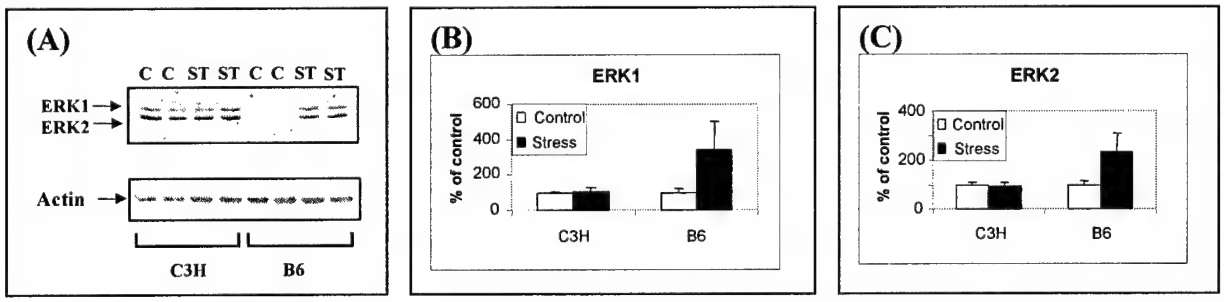

Figure 2. Effect of shear stress on phosphorylation levels of MAPK in osteoblasts isolated from C3H and B6 mice. Cells were subjected to fluid flow of 20 dynes/cm2 for 30 minutes. **(A):** Cell lysates were immunoblotted with anti-phospho-ERK and anti-actin antibodies. **(B&C):** The graph represents the densitometric measurements of ERK1 and ERK2 phosphorylation levels from western blots normalized by actin.

To further evaluate the involvement of the ERK-signaling pathway as to whether the protein kinase activity of ERK1 and/or 2 is essential for the fluid flow shear stress-induced osteoblast proliferation, we overexpressd dominant-negative constructs of ERK1 and ERK2 in

bone cells, and determined whether blocking the activation of the ERK1 and/or ERK2 would prevent the mechanical stress-induced bone cell proliferation.

Shear stress-induced cell proliferation was studied in human TE85 osteosarcoma cells that were transduced with MLV retroviral-based vectors expressing either the wild type (wt) or dominant negative, kinase-dead (kd) ERK1 and 2. Due to very low transduction efficiency in osteoblasts isolated from B6 mice, we used human TE85 cells in this part of the study as the transduction efficiency of TE85 cells is very high (79-90%). A HA tag was added to the N-terminus of each construct to help to distinguish the overexpressed enzyme from the endogenous enzyme. In order to distinguish the overexpressed ERK2 from the endogenous protein, a tag of 35 amino acids in size was introduced to the C-terminus of the protein. An MLV-red fluorescent protein (RFP) vector was also included as a control for comparison.

To ascertain that the wild-type ERK expression vectors expressed functionally active ERK1 and ERK2, and that the kinase-dead mutants of ERK vectors expressed inactive ERK1 and ERK2, protein kinase activity was assayed. As shown in Figure 3, ERK1 and ERK2 expressed by each corresponding wild-type expression vector (E1 and E2) were active as a MAPK whereas ERK1 and ERK2 expressed by each corresponding kinase-dead expression vector (e1 and e2) were completely inactive as a MAPK. Furthermore, the results here also suggest that the addition of a 35 amino acid tag at the C-terminus did not appear to have any effect on the protein kinase activity of ERK2.

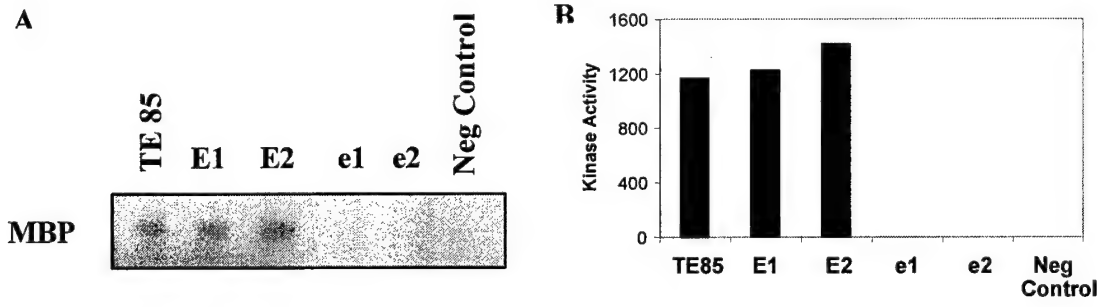

Figure 3. The Protein kinase activity of protein products expressed by each ERK expression vector. **(A):**To ascertain that the wild-type ERK expression vectors expressed functionally active ERK1 and ERK2, respectively, and that the kinase-dead mutants of ERK vectors expressed inactive ERK1 and ERK2, respectively, the corresponding ERK in lysates of *E. coli* expressing wild type GST-ERK1 and GST-ERK2 vectors (E1 and E2, respectively) or that of *E. coli* expressing kinase-dead GST-ERK1 and ERK2 vectors (e1 and e2, respectively) were isolated with glutathione-conjugated beads. The protein kinase assay was then assayed with MBP as the substrate. A negative control (lysates of E. coli without the ERK construct) and TE85 cell lysate (positive control) were included for comparison. **(B):**The graph represents the densitometric measurements of kinase activity.

Human TE85 osteosarcoma cells were transduced three times with each of the test retroviral vectors with a total MOI of 30. To ensure that human TE85 cells transduced with ERK expressing MLV vectors indeed overexpress corresponding ERKs, we measured the protein level of overexpressed (oERK1 and oERK2, respectively) and endogeneous (eERK1 and eERK2) ERK1 and 2 in cell lysates of transduced TE85 cells. As shown in Figure 4, TE85 cells transduced with MLV vectors expressing either wild type or kinase-dead mutants of ERK1 or 2 led to overexpression of ERK1 and ERK2 protein, respectively.

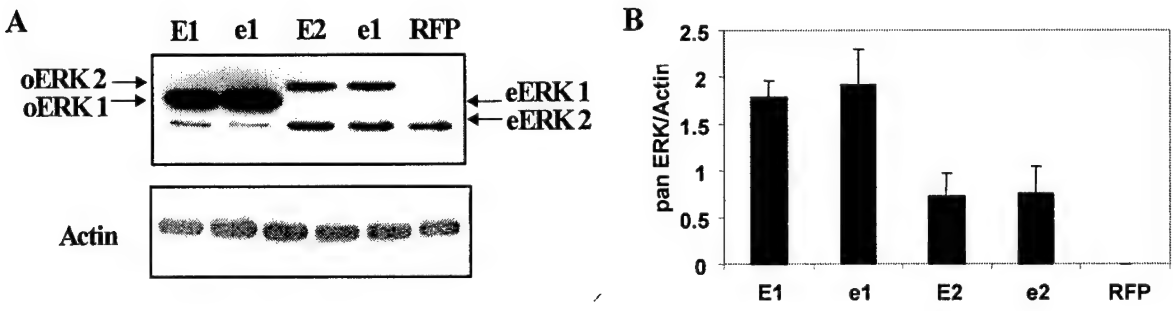

Figure 4. Overexpression of ERK proteins in human TE85 cells transduced with MLV vectors expressing wild-type (E1 and E2) or kinase-dead mutants (e1 and e2) of ERK. (A): To ensure that human TE85 cells transduced with ERK expressing MLV vectors indeed overexpress corresponding ERKs, the protein level of overexpressed (oERK1 and oERK2, respectively) and endogeneous (eERK1 and eERK2) ERK1 and 2 was measured in cell lysates of TE85 cells transduced with respective MLV vectors by western blot analysis. The oERK2 has an extra 35 aa at the C-terminus compared to eERK2. Cells transfected with MLV-RFP vector were included as a negative control. The blot was stripped and reblotted with anti-actin antibody to assess the protein loading.**(B):** The graph represents the densitometric measurements of ERK1 and ERK2 expression levels from western blots normalized by actin.

To test whether the protein kinase activity of ERK1 and/or ERK2 is essential for the fluid flow shear stress-induced proliferation of osteoblasts, we determined the effect of overexpression of kinase-dead ERK1 (e1) or ERK2 (e2) on [^{3}H]thymidine incorporation in response to shear stress. Figure 5 shows that TE85 cells exhibited a significant (~2-fold) increase in cell proliferation in response to a 30-min steady 20 dynes/cm^2 shear stress. Furthermore, overexpression of either wild type ERK1 or ERK2 resulted in a similar increase in cell proliferation in response to shear stress as compared to the controls. On the other hand, either a dominant-negative, kinase-dead ERK1 (e1) or ERK2 (e2) mutant completely blocked the mitogenic response of TE85 cells to the shear stress, suggesting that ERK1 and ERK2 each have an important role in mediating the shear stress-induced bone cell proliferation. Figure 5 also shows that MLV-RFP showed a similar response to shear stress as normal TE85 cells thus indicating that transfection of TE85 cells with the MLV vector did not affect the bone cell mitogenic response of these cells to the 30-min shear stress.

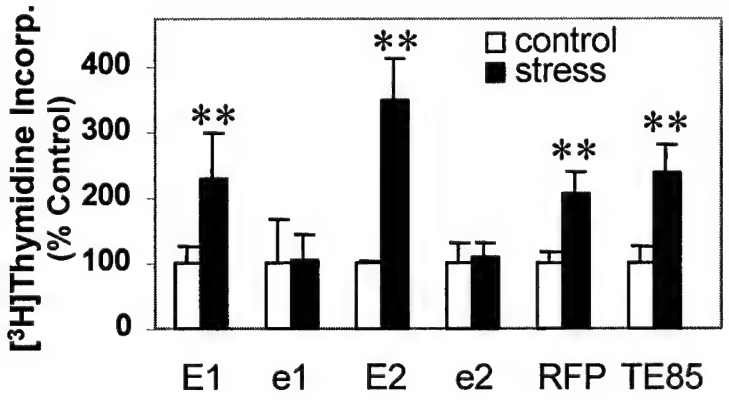

Figure 5: Effect of overexpression of ERK1 (E1 and e1) or ERK2 (E2 and e2) on the shear stress-induced increase in [^{3}H]thymidine incorporation. To test whether the protein kinase activity of ERK1 and/or ERK2 is essential for the fluid flow shear stress-induced proliferation of osteoblasts, we determined the effect of overexpression of kinase-dead ERK1 (e1) or ERK2 (e2) on [^{3}H]thymidine incorporation in response to shear stress. * *$p<0.01$.

These results clearly show that the protein kinase activity of both ERK1 and ERK2 is essential for the fluid flow shear stress-induced osteoblast proliferation. The most intriguing finding of this study is that overexpressing of an inactive form of ERK1 or ERK2 alone is sufficient to block the actions of endogenous ERKs in response to flow shear stress in bone cell proliferation.

Specific Objective 2: Evaluate changes in gene expression of those genes known to be involved in mediating loading signal using in-house microarray.

In order to study the genes involved in the mechanical signaling pathway, we applied the microarray technique. Our hypothesis is that the expression level of the genes involved in the mechanical signaling would be higher in the B6 mice as compared to C3H mice since B6 mice are responsive to mechanical stress whereas C3H mice do not respond to mechanical loading. Thus, to study the genetic basis for difference in loading signal in response to shear stress between C3H and B6 mice strains, we identified the genes in which the expression level increased more than two-fold when subjected to shear stress as compared to no stress in these two strains. The bone cells isolated from B6 and C3H mice were subjected to fluid flow shear stress of 20 dynes/cm^2 for 30 minutes. After 4 hours, RNA was extracted and microarray was performed.

Significantly Increased or Decreased Gene Expression from B6 Osteoblasts After Sheer Stress (Tables 1 & 2)

Table 1. List of genes in which expression level increased more than two-fold after application of shear stress as compared to control cells isolated from B6 mice. The ratios for the microarray were determined by using Genespring software.

Accession #	Fold Change	Gene Name
C81354	6.021867	
X15848	3.62071	Retinoic acid receptor gamma
J04113	3.536071	Mouse thyroid hormone receptor (NUR/77)
AF013170	3.508688	TNF related ligand TRANCE
TC159688	3.315779	Mus musculus IGFBP5 mRNA, complete cds
X05010	3.117075	Colony stimulating factor alpha (TNFa) gene
AU024669	3.105589	
M69293	3.028576	Mouse Id2 protein (Id-2)
E04743	2.992537	Mouse IL-1 alpha
X57796	2.960955	Mouse 55-kda tumor necrosis factor receptor
J00370	2.927765	Mouse c-fos gene; cellular homolog to viral oncogene
J05265	2.894687	Interferon gamma receptor
U64331	2.887784	Mouse Osteoprotegerin (OPG)
AF009011	2.781368	axin
AB015978	2.778422	Mouse Oncostatin M receptor beta

U81451	2.773452	Estrogen receptor beta (ESTRB)
M28021	2.752648	Mouse Homeo domain protein (HOX 1.3)
C78332	2.727276	
M59929	2.726371	Signal-trans. guanine nuleotide-binding protein (GNA01)
U58503	2.682652	Keratinocyte growth factor/fibroblast growth factor-7
E01057	2.672017	Mouse interleukin-1(IL-1) precursor
D49438	2.64229	Mouse 25-hydroxyvitamin D3 24-hydroxylase
X56848	2.610531	Bone morphogenetic protein 4 (BMP-4)
AF053713	2.600324	Mouse Osteoprotegerin ligand
AJ009862	2.584103	Transforming growth factor-beta 1
L35303	2.571284	TNF receptor associated factor 2 (TRAF2)
L0253F11-3	2.566142	Mus musculus orphan nuclear hormone receptor (CAR) gene, complete sequence
L28108	2.553446	Mouse PTH/PTHrP
L0065H09-3	2.529236	Homo sapiens ribosomal protein S21 (RPS21), mRNA
TC201479	2.526702	Homo sapiens MEBP-1 mRNA for MAPK-ERK binding protein-1, complete cds
TC175431	2.519852	
D89628.1	2.506003	Vascular endothelial growth factor D (VEGF-D)
BB500047	2.498375	beta-catenin
U39060	2.49294	Glucocorticoid receptor interacting protein 1 (GRIP1)
U36384	2.488445	Mouse twist-related bHLH protein Dermo-1
TC157862	2.438857	Homo sapiens mRNA; cDNA DKFZp586C1620 (from clone DKFZp586C1620); partial cds
U85259	2.437383	Estrogen related receptor alpha (ESTRRA)
X15202	2.428389	Fibronectin Receptor beta-chain (VLA5-homolog.)
M89798	2.414296	Mouse WNT-5a
U51001	2.398422	DLX-1 gene
SU78076	2.394921	Mouse sepiaterin reductase gene
SJ00357	2.394785	Mouse alpha amylase-2 gene
U78048	2.38784	Bone morphogenetic protein type II receptor BRK-3
D16250.1	2.37863	Mouse BMP receptor
AF019048	2.370698	Mouse RANKL
TC200632	2.360679	Homo sapiens CCR4-NOT transcription complex, subunit 8 (CNOT8), mRNA
AF068615	2.358135	Ciliary neutotrophic factor receptor alpha precursor
NM_010703	2.355529	Lef 1
X76401	2.340111	Tumor necrosis factor receptor 2
J04069	2.338559	Insulin-like growth factor II (IGF-II)
SU96809	2.333815	Mouse chromatin structural protein homolog gene
TC177706	2.332596	
C78942	2.326618	
C80859	2.321968	
V00727	2.315034	c-fos oncogene
D17630	2.31364	Mouse mRNA for interleukin-8 receptor
TC187351	2.313193	Homo sapiens actin related protein 2/3 complex, subunit 4 (20 kD) (ARPC4), mRNA
D31942	2.295312	Mouse Oncostatin M
AF179369	2.28034	Insuline-like growth factor binding protein 5 protease
C85074	2.27293	
TC202099	2.258783	
E03515	2.257122	Mouse interleukin 6 receptor protein
J04766.1	2.254782	Plasminogen

L0029F01-3	2.248046	
Y15800	2.242617	Mouse mRNA for G-protein coupled receptor kinase 6-D
L0051E10-3	2.22982	Mus musculus fibrillarin (Fbl), mRNA
C76615	2.224257	
TC188980	2.223752	
TC186487	2.210573	Mus musculus (clone Clebp-1) high mobility group 1 protein (HMG-1)mRNA,complete cds
TC161819	2.210151	
L12447	2.194287	Insuline-like growth factor binding protein 5 (IGFBP5)
TC186750	2.191918	Mus musculus protein tyrosine phosphatase 4a1 (Ptp4a1), mRNA
M92416	2.191191	Fibroblast growth factor (FGF6)
TC166114	2.186043	Mouse mRNA for ELP3, complete cds
M29464	2.179255	Mouse platelet-derived growth factor a chain (PDGA)
TC160957	2.176756	
TC162199	2.171346	Mus musculus PL-6 (Pl6), mRNA
TC186822	2.155771	Homo sapiens splicing factor (CC1.3) (CC1.3), mRNA
C81425	2.154317	
X53802	2.150552	Mouse mRNA for interleukin-6 receptor
TC176196	2.149525	
SM95800	2.14905	Mouse Myogenin gene
TC160277	2.138307	Mus musculus 15 kDa selenoprotein (Sep15) mRNA, complete cds
TC201280	2.131578	Mus musculus D-dopachrome tautomerase gene, complete cds
J04953	2.129044	Gelsolin gene
TC186937	2.125651	Mus musculus DBA/2J delta proteasome subunit gene, complete cds
AF067191	2.124936	Fibroblast growth factor 1.a gene, exon 1
TC188018	2.116157	
TC174028	2.107252	Mus musculus spermidine/spermine N1-acetyl transferase (Sat), mRNA
TC160410	2.089787	Mus musculus serum and glucocorticoid-dependent protein kinase (Sgk)mRNA
TC175783	2.08736	Mus musculus hyaluronidase 2 (Hyal2), mRNA
H3147A10	2.081017	
TC187978	2.074785	Mus musculus recombining binding protein suppressor of hairless(Drosophila)(Rbpsuh)
AF120489	2.073418	Growth hormone receptor/growth hormone-binding protein
M63650	2.071397	Mouse M-twist gene
TC174003	2.070687	Mus musculus kidney predominant protein NCU-G1 (NCU-G1), mRNA
TC174701	2.069076	Homo sapiens JTV1 gene (JTV1), mRNA
TC200417	2.060727	Human gene for dihydrolipoamide succinyltransferase, complete cds (exon 1-15)
TC173360	2.057717	Homo sapiens actin related protein 2/3 complex, subunit 5 (16 kD) (ARPC5), mRNA
AF075717	2.044671	Transforming growth factor beta 1-induced factor 2
TC199965	2.043639	Homo sapiens cDNA FLJ14219 fis, clone NT2RP3003800, highly similar to Rattus norveg
TC162168	2.041731	Homo sapiens CGI-147 protein (LOC51651), mRNA
C80763	2.038737	
AU022524	2.028801	
X58636.1	2.025792	(LEF1) lymphoid enhancer binding factor 1
H3120A04	2.021601	
C86855	2.018469	Mus musculus scmh1 mRNA for sex comb on midleg homolog protein, complete cds
L32751	2.013074	Mouse (Clone M1) GTPase (RAN)
AA119293	2.012701	small inducible cytokine A6
TC186472	2.00335	Mouse t-complex protein (Tcp-1x) mRNA, 3' end
TC201234	2.000614	Rattus norvegicus lamina associated polypeptide 1C (LAP1C) mRNA, complete cds

Table 2. List of genes in which expression level decreased more than two-fold after application of shear stress as compared to control cells isolated from B6 mice. The ratios for the microarray were determined by using Genespring software.

Accession #	Fold Change	Gene Name
TC163213	6.323833	
TC186806	4.749427	Homo sapiens apoptosis-related protein PNAS-3 (PNAS-3) mRNA, partial cds
C79115	4.397889	
C87796	4.207526	
TC177345	4.145114	Homo sapiens hypothetical protein FLJ10761 (FLJ10761), mRNA
TC193180	3.797844	Mus musculus tyrosine hydroxylase (Th), mRNA
TC167104	3.656022	
C80790	3.562263	
C79008	3.479888	
TC160201	3.372998	Homo sapiens mRNA; cDNA DKFZp586A0722 (from clone DKFZp586A0722)
TC176539	3.316524	Mus musculus small GTP-binding protein RAB25 (Rab25) gene, complete cds
TC190432	3.315813	
TC173689	3.286380	Mus musculus putative CCAAT binding factor 1 (mCBF) mRNA, mCBF1, complete cds
TC176094	3.229843	Homo sapiens KIAA0205 gene product (KIAA0205), mRNA
TC159792	3.224493	Homo sapiens ribosomal protein S9 (RPS9), mRNA
L0298F03-3	3.224286	
AU019373	3.178850	
C86899	3.094014	
TC202698	3.087886	Homo sapiens zinc finger protein 198 (ZNF198), mRNA
TC158511	3.063481	Homo sapiens mRNA;cDNA DKFZp586P0123 (from clone DKFZp586P0123);partial cds
L0069G07-3	3.044982	Homo sapiens hypothetical protein FLJ10579 (FLJ10579), mRNA
TC174040	3.028745	
TC188831	3.027351	Homo sapiens small nuclear ribonucleoprotein polypeptide F (SNRPF), mRNA
TC178609	3.017881	Mus musculus nuclear RNA export factor 1 homolog (S. cerevisiae) (Nxf1), mRNA
TC204210	3.013675	Homo sapiens B-cell CLL/lymphoma 9 (BCL9), mRNA
TC208948	3.009861	Mus musculus Janus kinase 2 (Jak2), mRNA
AU024699	2.999606	
C81530	2.965025	
AU022331	2.935256	
TC204243	2.907804	Homo sapiens mRNA for KIAA1524 protein, partial cds
TC175962	2.872361	Homo sapiens clone CTB-10G5, complete sequence
TC189875	2.871053	Homo sapiens hypothetical protein FLJ11110 (FLJ11110), mRNA
TC162398	2.857831	Homo sapiens insulin receptor tyrosine kinase substrate (LOC55971), mRNA
L0223G04-3	2.835623	
TC161135	2.828019	Homo sapiens cDNA FLJ14228 fis, clone NT2RP3004148
TC163534	2.797985	
TC190975	2.791493	Homo sapiens centrosomal P4.1-associated protein (CPAP) mRNA, complete cds
AU020234	2.767904	Homo sapiensTRPM-2,cytosolic epoxide hydrolase,nicotinic acetylcholine receptor alpha
C87530	2.755052	
L0226E04-3	2.734502	Homo sapiens LIM domain only 7 (LMO7), mRNA

TC202077	2.674004	
TC191546	2.673286	Homo sapiens cDNA FLJ12145 fis, clone MAMMA1000395
C80806	2.666355	
TC178272	2.665531	Homo sapiens cDNA FLJ13303 fis,clone OVARC1001372,highly similar to Homo sapien
C81384	2.663685	Homo sapiens KIAA0042 gene product (KIAA0042), mRNA
L0051A02-3	2.622076	Homo sapiens heterogeneous nuclear ribonucleoprotein A0 (HNRPA0), mRNA
H3129D12	2.609591	
TC163806	2.601031	Homo sapiens heat shock transcription factor 2 binding protein (HSF2BP), mRNA
TC157219	2.574551	Homo sapiens eukaryotic protein synthesis initiation factor mRNA, complete cds
C81435	2.564388	
TC187187	2.547066	Homo sapiens mRNA; cDNA DKFZp761M2324 (from clone DKFZp761M2324)
TC189163	2.544920	Homo sapiens cDNA: FLJ23321 fis, clone HEP12396
C78157	2.535713	
L0290G10-3	2.516292	Homo sapiens KIAA0738 gene product (KIAA0738), mRNA
TC157805	2.512923	Homo sapiens GTP-binding protein (NGB), mRNA
TC173604	2.511347	Homo sapiens loss of heterozygosity, 11, chromosomal region 2, gene A (LOH11CR2A)
TC210779	2.507478	Homo sapiens KIAA0513 gene product (KIAA0513), mRNA
TC159887	2.492242	Homo sapiens KIAA0005 gene product (KIAA0005), mRNA
TC188500	2.489737	Homo sapiens mRNA for repressor protein, partial cds
TC160230	2.480316	Homo sapiens mRNA; cDNA DKFZp566J151(from clone DKFZp566J151);complete cds
TC174370	2.479888	Mus musculus solute carrier family 34 (sodium phosphate), member 2 (Slc34a2), mRNA
NM-008513	2.473082	LRP5 #6
TC178738	2.470564	
TC176946	2.458136	Homo sapiens hypothetical protein FLJ20241 (FLJ20241), mRNA
TC189678	2.452885	Homo sapiens mRNA for KIAA0693 protein, partial cds
TC161711	2.422831	Homo sapiens nesca protein (NESCA), mRNA
TC186798	2.416530	Homo sapiens hypothetical protein FLJ10488 (FLJ10488), mRNA
TC188265	2.399167	Homo sapiens Sec31 protein mRNA, complete cds
TC206463	2.385723	
C86942	2.350195	
TC204786	2.340445	Homo sapiens SWI/SNFrelated,matrix associated,actin dependent regulator of chromati
TC174182	2.333507	Mus musculus platelet-activating factor acetylhydrolase, isoform 1b,(Pafah1b3), mRNA
S67455	2.324881	Osteocalsin
TC163121	2.321306	Homo sapiens cDNA FLJ12969 fis, clone NT2RP2005841
TC176186	2.298626	Homo sapiens LIM and cysteine-rich domains 1 (LMCD1), mRNA
L0291D11-3	2.279614	
L0013H08-3	2.278326	Homo sapiens eukaryotic translation elongation factor 1 gamma (EEF1G), mRNA
TC190732	2.274502	Homo sapiens cDNA: FLJ21020 fis, clone CAE06067
TC192702	2.261900	
EST03087	2.260475	
TC177370	2.242102	Human Tcr-C-delta gene,exons 1-4; Tcr-V-delta gene,exons 1-2 Tcr-C-alpha gene, exor
TC176521	2.238748	Homo sapiens KIAA0615 gene product (KIAA0615), mRNA
TC159038	2.221344	Homo sapiens mRNA; cDNA DKFZp761E212 (from clone DKFZp761E212)
TC201917	2.219296	Homo sapiens cDNA FLJ12783 fis, clone NT2RP2001876
TC191320	2.217481	Rattus norvegicus gene for T cell receptor eta chain, partial cds
AU022414	2.214434	Homo sapiens KIAA0940 protein (KIAA0940), mRNA
TC160509	2.214421	Homo sapiens diaphorase (NADH) (cytochrome b-5 reductase) (DIA1), mRNA
C85917	2.205803	Homo sapiens spinocerebellar ataxia 1

TC190467	2.199626	Homo sapiens cDNA FLJ13645 fis, clone PLACE1011310
TC203547	2.198232	Homo sapiens cDNA FLJ12642 fis, clone NT2RM4001965
TC160176	2.198150	Homo sapiens mRNA for KIAA1470 protein, partial cds
TC161597	2.194239	
TC202599	2.181680	Homo sapiens KIAA0244 protein (KIAA0244), mRNA
TC190059	2.174398	Homo sapiens transmembrane 4 superfamily member(tetraspan NET-7) (NET-7),mRNA
TC157266	2.169345	Mus musculus macrophage galactose N-acetyl-galactosamine specific lectin(Mgl),mRN/
TC199932	2.167705	Homo sapiens MADS box transcription enhancer factor2, polypeptide B (MEF2B),mRNA
TC161470	2.163998	Homo sapiens mRNA; cDNA DKFZp434E0121 (from clone DKFZp434E0121)
TC163446	2.158835	Mus musculus murinoglobulin 1 (Mug1), mRNA
TC178608	2.158464	Homo sapiens 8q22.1 region and MTG8 (CBFA2T1) gene, partial cds
L0261D05-3	2.158177	Homo sapiens similar to phosphorylase kinase, alpha 2 (liver) (H. sapiens) (LOC63600)
TC190403	2.152387	Homo sapiens G-protein-coupled receptor induced protein GIG2 (GIG2) mRNA
TC167570	2.146512	Mus musculus citrin (Slc25a13) mRNA, complete cds
TC157243	2.139440	Homo sapiens myosin IC (MYO1C), mRNA
TC158841	2.133129	Homo sapiens cDNA FLJ13924 fis, clone Y79AA1000540
TC160307	2.131873	Homo sapiens isocitrate dehydrogenase 3 (NAD+) alpha (IDH3A), mRNA
TC176029	2.128533	Homo sapiens mRNA; cDNA DKFZp434L1850(from clone DKFZp434L1850);partial cds
L0221A07-3	2.125280	
C81146	2.119302	
TC160464	2.116825	Homo sapiens mRNA-associated protein mrnp41 mRNA, complete cds
TC202524	2.112259	Human TFIID subunits TAF20 and TAF15 mRNA, complete cds
TC189397	2.096525	Homo sapiens hypothetical protein (FLJ20323), mRNA
TC189007	2.094517	Mus musculus RAD50 homolog (S. cerevisiae) (Rad50), mRNA
TC188371	2.094454	Human clone 23721 mRNA sequence
TC188050	2.093248	Homo sapiens MDS017 (MDS017) mRNA, complete cds
C78068	2.078961	
TC163941	2.074859	
TC204346	2.066088	Homo sapiens cDNA: FLJ22573 fis, clone HSI02387
AU019250	2.063553	Homo sapiens T-box 19 (TBX19), mRNA
L0215A02-3	2.058678	
TC200441	2.047412	Homo sapiens guanine nucleotide binding protein (G protein), (GNAI3), mRNA
TC191257	2.044590	Human IGF-I mRNA for insulin-like growth factor I
TC187210	2.040991	Homo sapiens cDNA FLJ13872 fis, clone THYRO1001322
TC173819	2.035938	Homo sapiens thyroid receptor interactor (TRIP3) mRNA, 3' end of cds
C76739	2.032122	Mus musculus macrophage C-type lectin (Mpcl), mRNA
AU019952	2.032041	Homo sapiens mRNA for KIAA0597 protein, partial cds
AU041136	2.027832	Bacteriophage lambda, complete genome
TC188786	2.026039	Rattus norvegicus NADH/NADPH mitogenic oxidase subunit p65-mox mRNA
AU024767	2.024597	Mus musculus mRNA for PC3B protein
L0290B05-3	2.023050	
TC160773	2.020360	M.musculus DNA 3'flanking minisatellite transgene 110C
AU019202	2.015859	Homo sapiens MSTP046 mRNA, complete cds
TC204088	2.015016	Homo sapiens HYA22 protein (HYA22), mRNA
AU022194	2.010488	
TC163812	2.010332	Homo sapiens cDNA FLJ10366 fis, clone NT2RM2001420
TC164591	2.009105	M.musculus mRNA for intestinal tyrosine kinase
TC176191	2.008425	Homo sapiens BM022 protein (BM022), mRNA

AU024701	2.008356	
TC203734	2.000904	Homo sapiens mRNA for KIAA1302 protein, partial cds
C78087	2.000170	

As shown in Table 1, there are 109 genes that show more than two-fold increase in expression in cells subjected to fluid flow shear stress as compared to the non-stressed cells in B6 mice. Table 2 shows that there are 139 genes that show more than two-fold decrease in expression in stressed cells as compared to the non-stressed cells in B6 mice.

Significantly Increased or Decreased Gene Expression in C3 Osteoblasts After Sheer Stress (Tables 3 & 4)

Table 3. List of genes in which expression level increased more than two-fold after application of shear stress as compared to control cells isolated from C3H mice. The ratios for the microarray were determined by using Genespring software.

Accession #	Fold Change	Gene Name
M69293	5.342443	Mouse Id2 protein (Id-2)
AF179369	4.480995	Insuline-like growth factor binding protein 5 protease
M63650	4.314368	Mouse M-twist gene
D16250.1	4.153827	Mouse BMP receptor
M89798	3.86404	Mouse WNT-5a
U85259	3.828085	Estrogen related receptor alpha (ESTRRA)
AF056187	3.623736	Insulin-like growth factor I receptor
AF126159	3.500622	Mouse big MAP kinase 1a (BMK1), mRNA
X57413	3.49456	Transforming growth factor-beta 2
L27424	3.46014	Mouse metalloproteinase inhibitor TIMP-3)
U39060	3.454962	Glucocorticoid receptor interacting protein 1 (GRIP1)
U58503	3.376605	Keratinocyte growth factor/fibroblast growth factor-7
AJ009862	3.354771	Transforming growth factor-beta 1
D17630	3.210925	Mouse mRNA for interleukin-8 receptor
U67610	3.206105	Fibroblast growth factor 1 (FGF-1)
X05010	3.13227	Colony stimulating factor alpha (TNFa) gene
AB015978	3.128478	Mouse Oncostatin M receptor beta
M92416	3.113992	Fibroblast growth factor (FGF6)
AB009993	3.08771	Collagen A1(V)
M97017	3.059502	Osteogenic protein-2 (OP-2)
L25602.1	3.019166	Mouse morphogenetic protein 2 (BMP-2) gene
X67348	3.012249	COL10A1 gene for alpha - collagen type x
X15202	2.947969	Fibronectin Receptor beta-chain (VLA5-homolog.)
J00370	2.937989	Mouse c-fos gene; cellular homolog to viral oncogene
TC177706	2.931965	
U39545	2.926427	Bone morphogenetic protein 8b (BMP8b)
M59929	2.915431	Signal-trans. guanine nuleotide-binding protein (GNA01)
U70429	2.847221	Interleukin-4 induced gene-1 (FIG1)
U81451	2.841179	Estrogen receptor beta (ESTRB)

J04953	2.811038	Gelsolin gene
AB006034	2.796519	Mouse 25-hydroxyvitamin D3 1 alpha-hydroxylase
L32751	2.788244	Mouse (Clone M1) GTPase (RAN)
M29464	2.778772	Mouse platelet-derived growth factor a chain (PDGA)
L35303	2.759914	TNF receptor associated factor 2 (TRAF2)
AF020681	2.758174	Mouse core binding factor alpha1 sub unit isoform (Cbfa-1)
TC175431	2.745054	
D89628.1	2.738802	Vascular endothelial growth factor D (VEGF-D)
X14759	2.72283	Mouse Homeo box (HOX-7.1)
U64331	2.718682	Mouse Osteoprotegerin (OPG)
X57796	2.678408	Mouse 55-kda tumor necrosis factor receptor
D63644	2.6558	ARNT2 (F2#335)
E04743	2.655764	Mouse IL-1 alpha
TC200162	2.654953	Homo sapiens ribosomal protein L39 (RPL39), mRNA
X15848	2.650977	Retinoic acid receptor gamma
M28021	2.638262	Mouse Homeo domain protein (HOX 1.3)
TC173131	2.605621	Homo sapiens eukaryotic translation initiation factor 2,subunit 2(beta, 38kD)(EIF2S2)
AB021228.1	2.602641	Membrane-type 3 matrix metalloproteinase
TC173318	2.540124	Homo sapiens transmembrane trafficking protein (TMP21), mRNA
NM_010703	2.507729	Lef 1
J04113	2.482183	Mouse thyroid hormone receptor (NUR/77)
TC188890	2.457797	Mus musculus calponin 1 (Cnn1), mRNA
TC187062	2.448608	Homo sapiens 6.2 kd protein (LOC54543), mRNA
Perkin Elmer	2.425088	EST 91 from A.Thaliana
C86855	2.401036	Mus musculus scmh1 mRNA for sex comb on midleg homolog protein, complete cds
SU78076	2.395678	Mouse sepiaterin reductase gene
J05265	2.391902	Interferon gamma receptor
U36384	2.39182	Mouse twist-related bHLH protein Dermo-1
SM95800	2.381928	Mouse Myogenin gene
X62622	2.374983	(TIMP-2) Tissue inhibitor of metalloproteinases
TC158549	2.365563	
TC161819	2.363219	
TC190585	2.352407	
J04069	2.350386	Insulin-like growth factor II (IGF-II)
L0227G08-3	2.347008	Homo sapiens clone 82F9, complete sequence
L15436	2.336559	Isoform of TGF-b type II receptor
TC160410	2.316149	Mus musculus serum and glucocorticoid-dependent protein kinase (Sgk) mRNA
TC186487	2.30955	Mus musculus (clone Clebp-1) high mobility group 1 protein (HMG-1) mRNA
H3120A04	2.303708	
AF067191	2.290257	Fibroblast growth factor 1.a gene, exon 1
L28108	2.288727	Mouse PTH/PTHrP
TC187351	2.267528	Homo sapiens actin related protein 2/3 complex, subunit 4 (20 kD) (ARPC4), mRNA
L0011C07-3	2.266767	
TC201280	2.252388	Mus musculus D-dopachrome tautomerase gene, complete cds
AA253928	2.252074	endothelial monocyte
TC160692	2.249222	Homo sapiens myeloid leukemia factor 2 (MLF2), mRNA
H3124G02	2.242975	
C78676	2.236116	

AF026305	2.230761	Mouse Zinc finger transcription factor GLI
Y15800	2.227902	Mouse mRNA for G-protein coupled receptor kinase 6-D
TC160740	2.21674	Homo sapiens translocation protein 1 (TLOC1), mRNA
C78942	2.21332	
C87911	2.21322	Mus musculus SIL, MAP_17, CYP_a, SCL & CYP_b genes
X81582	2.210164	Insulin-like growth factor binding protein-4
TC191001	2.210023	Mus musculus transcription factor LRG-21 mRNA, complete cds
AF126063	2.209931	Connective tissue growth factor-like protein precursor
C81495	2.208941	
AA119293	2.203506	small inducible cytokine A6
TC159712	2.199665	Mus musculus RNA polymerase 1-1 (40 kDa subunit) (Rpo1-1), mRNA
TC159899	2.198992	
D31942	2.197945	Mouse Oncostatin M
TC173358	2.197787	Homosapienssignal sequence receptor,beta(translocon-associated protein beta)(SSR2)
C81364	2.179308	
TC160481	2.174184	Mus musculus calcium-binding protein Cab45a mRNA, complete cds
TC159868	2.173848	Mus musculus necdin (Ndn), mRNA
TC186472	2.169085	Mouse t-complex protein (Tcp-1x) mRNA, 3' end
TC186937	2.168598	Mus musculus DBA/2J delta proteasome subunit gene, complete cds
AU022429	2.168419	
C81299	2.167638	
TC161269	2.166696	Homo sapiens hypothetical protein FLJ20272 (FLJ20272), mRNA
C76825	2.154873	Mus musculus transient receptor potential-related protein (ChaK), mRNA
TC190469	2.149796	
TC201640	2.149553	Mus musculus arginine methyltransferase (Prmt2) mRNA, complete cds
AU024669	2.149365	
L0253F11-3	2.146557	Mus musculus orphan nuclear hormone receptor (CAR) gene, complete sequence
L0065E08-3	2.146445	
C78257	2.145905	Human mRNA for NADP dependent leukotriene b4 12-hydroxydehydrogenase,partial cds
AF009011	2.145423	axin
C87927	2.139591	
TC174006	2.135762	Homo sapiens asparaginyl-tRNA synthetase (NARS), mRNA
AF013170	2.135479	TNF related ligand TRANCE
X56848	2.13524	Bone morphogenetic protein 4 (BMP-4)
AA067193	2.131849	UDP-glucose dehydrogenase
TC174140	2.128732	Mus musculus Cdc42 GTPase-inhibiting protein (Cdgip-pending), mRNA
TC160359	2.125901	Homo sapiens clone RP11-486I22, complete sequence
D49438	2.125615	Mouse 25-hydroxyvitamin D3 24-hydroxylase
TC200023	2.119359	Mus musculus ribosomal protein L27 (Rpl27), mRNA
TC174370	2.117575	Mus musculus solute carrier family 34 (sodium phosphate), member 2 (Slc34a2), mRNA
C86037	2.107628	
BB500047	2.099311	beta-catenin
L0041A01-3	2.090664	
C78966	2.077118	
L0065H09-3	2.074872	Homo sapiens ribosomal protein S21 (RPS21), mRNA
C78958	2.068447	
TC189109	2.065315	Mus musculus transcription elongation factor B (SIII), polypeptide 3 (110kD) (Tceb3)
TC181404	2.061944	

TC160525	2.06007	Homo sapiens cDNA: FLJ21894 fis, clone HEP03434
L0029F01-3	2.059959	
L0008A03-3	2.048002	
TC201527	2.047403	Homo sapiens from HeLa cyclin-dependent kinase 2 interacting protein (CINP), mRNA
TC187519	2.047178	
TC157688	2.046966	Mus musculus hematological and neurological expressed sequence 1 (Hn1), mRNA
TC173042	2.03422	Homo sapiens NADH-ubiquinone dehydrogenase 1 beta subcomplex mRNA, complete cc
U78048	2.028893	Bone morphogenetic protein type II receptor BRK-3
AU040912	2.02622	
TC157249	2.020829	Homo sapiens mRNA for KIAA0622 protein, partial cds
TC160904	2.015319	
C76812	2.013664	
TC160230	2.011371	Homo sapiens mRNA; cDNA DKFZp566J151 (from clone DKFZp566J151); complete cds
SJ00357	2.00887	Mouse alpha amylase-2 gene
TC159122	2.007755	Homo sapiens clone RP11-359J14, complete sequence
C81549	2.005677	
TC157612	2.002072	Mus musculus thioredoxin reductase 1 (Txnrd1), mRNA
X76401	2.001228	Tumor necrosis factor receptor 2

Table 4. List of genes in which expression level decreased more than two-fold after application of shear stress as compared to control cells isolated from C3H mice. The ratios for the microarray were determined by using Genespring software.

Accession #	Fold Change	Gene Name
L0003B11-3	7.251633	Homosapiens FRA3B common fragile region,diadenosine triphosphate hydrolase (FHI
C81354	5.150292	
AU024549	4.566669	
C86942	4.135808	
TC161706	3.814792	
AU023208	3.674891	Mus musculus guanine nucleotide binding protein, alpha 14 (Gna14), mRNA
TC203078	3.630153	
TC169364	3.333058	
AU019631	3.262583	
TC158443	3.253914	
AU040173	3.189639	
TC173754	3.153296	Mus musculus DAZ-like putative RNA binding protein mRNA, complete cds
TC187226	3.104026	Mus musculus EST from clone 1498755, 3' end
AU040981	2.964905	
TC171051	2.935193	
C78087	2.929459	
EST03087	2.875889	
TC162350	2.870055	Mus musculus UDP-N-acetyl-alpha-D-galactosamine:polypeptideN- 3 (Galnt3), mRNA
TC160175	2.781838	Mus musculus serine/threonine kinase receptor associated protein (Strap), mRNA

TC208960	2.779201	
TC174179	2.777212	Mus musculus nuclear transcription factor RelA (Rela) gene, complete cds
TC188305	2.769935	
TC178738	2.715629	
C78068	2.696100	
C87638	2.679857	
TC157385	2.675020	Mus musculus Ena-VASP-like isoform (Evl1)mRNA, complete cds,alternatively spliced
AU041329	2.651487	
L0208A04-3	2.645424	
AU021860	2.603490	
AU022194	2.598836	
NM_007561	2.594891	Huamn BMP2/4
TC173759	2.577267	
AU022374	2.566131	
TC174791	2.531756	Mus musculus X transporter protein 3 (Xtrp3), mRNA
C80763	2.498239	
TC173399	2.490726	Mus musculus signal sequence receptor, delta (Ssr4), mRNA
H3126E09	2.477740	
AU021733	2.463330	
TC162016	2.459140	Mus musculus X-linked lymphocyte-regulated 3b (Xlr3b), mRNA
C78061	2.443694	
C86825	2.440315	
C78093	2.437616	
AU022156	2.435370	
TC162632	2.404160	Rattus norvegicus bHLH transcription factor Mist1 (Mist1) gene, complete cds
AU022430	2.385197	
C78157	2.374702	
EST03029	2.366326	
TC189251	2.343817	Homo sapiens KIAA0553 protein gene, complete cds;and alphaIIb protein gene
C86821	2.323865	
TC173324	2.310638	Psammomys obesus beacon mRNA, complete cds
TC205126	2.306227	
AU022065	2.303341	
AU021745	2.299328	
AU023256	2.296894	
TC192702	2.288848	
C79008	2.271746	
AU022321	2.270753	
EST03446	2.263182	Rattus norvegicus mRNA for dihydrolipoamide acetyltransferase
C76575	2.262311	
AU022331	2.262090	
AU024767	2.257646	Mus musculus mRNA for PC3B protein
TC198946	2.241669	
TC187710	2.233919	Mus musculus mRNA for hypothetical protein expressed in thymocytes), partial
TC172405	2.224768	
TC188356	2.222745	
TC186921	2.220592	Mus musculus U22 snoRNA host gene (UHG) gene, complete sequence
EST03496	2.214832	

TC174040	2.198529	
TC203464	2.194281	Mus musculus caspase 12 (Casp12), mRNA
L0219C11-3	2.191261	
TC163941	2.189350	
TC165384	2.187309	Homo sapiens sciellin (SCEL), mRNA
AU022363	2.185691	
C87602	2.178928	
AU024748	2.175758	
AU021952	2.163344	
C80899	2.161401	
TC200616	2.160273	Mus musculus gene rich cluster, C8 gene (Grcc8), mRNA
NM_019305	2.156498	Human FGF2
AU024596	2.154303	
TC163888	2.146388	Mouse integrin beta 4 subunit mRNA
AU023218	2.144509	
EST02095	2.142997	
AU023189	2.140748	
NM_013414	2.139277	Rat OSTEOCALCIN
AU024605	2.137971	
TC165048	2.137789	
TC160424	2.136576	Homo sapiens E-1 enzyme (MASA), mRNA
C78176	2.112627	
AU043475	2.109897	
AU024499	2.106700	
AU024601	2.104568	
TC188478	2.103129	
AU021766	2.096848	
AU022382	2.096010	
TC202511	2.088855	Mus musculus Pro-rich, PH, SH2 domain-containing signaling mediator (PSM) mRNA
AU022202	2.086047	
TC166103	2.081321	
TC202623	2.079226	
C86859	2.078406	Homo sapiens, clone hRPK.58_A_1, complete sequence
TC166162	2.067844	
EST03382	2.067519	Mus musculus transthyretin (Ttr), mRNA
TC208089	2.065965	
TC161597	2.065945	
TC205477	2.064887	Mus musculus potassium voltage-gated channel,subfamily H(eag-related),(Kcnh1)
TC186112	2.063845	
TC204141	2.062597	Rattus norvegicus mevalonate pyrophosphate decarboxylase mRNA, complete cds
TC197087	2.057604	
AU022204	2.056734	
AU022409	2.055760	
TC192594	2.053742	
EST03436	2.046538	
TC202525	2.043880	Rattus norvegicus hypertension-related calcium-regulated gene mRNA, complete cds
TC210779	2.042810	Homo sapiens KIAA0513 gene product (KIAA0513), mRNA
AU022341	2.042184	

AU022070	2.042046	
AU024727	2.041442	
AU043452	2.036570	
TC188626	2.035291	M.musculus mRNA for arachidonate epidermis-type 12(S)-lipoxygenase
EST03723	2.032456	
AU022460	2.029631	
TC160632	2.028687	Mus musculus cullin 1 (Cul1) mRNA, complete cds
Z46629.1	2.027188	Rat SOX 9
TC205634	2.024558	Mus musculus bone morphogenetic protein 15 (Bmp15), mRNA
TC201670	2.024546	Mus musculus homer-2b mRNA, complete cds
AU022330	2.024488	
TC161617	2.022511	Mus musculus beta-1,4-galactosyltransferase VI mRNA, complete cds
AU024594	2.021603	Mus musculus mRNA for cysteinyl-tRNA-synthetase (CysRS)
C81146	2.016730	
TC203654	2.008460	
TC161681	2.007609	
C87514	2.003433	
TC188237	2.002615	Mus musculus fragile X mental retardation syndrome 1 homolog (Fmr1), mRNA
TC174887	2.000214	Mus musculus solute carrier family 12, member 2 (Slc12a2), mRNA

As shown in Table 3, there are 142 genes that are upregulated in cells subjected to fluid flow shear stress as compared to the non-stressed cells in C3H mice. There are 134 genes that are downregulated in stressed vs. non-stressed cells in these mice (Table 4).

Comparison of gene expression profiles between B6 and C3H mice.

Since our main objective is to find out the genes involved in the mechanical signaling, we compared the gene expression profiles between B6 and C3H. A combined list of B6S/B6C and C3HS/C3HC was made to compare B6S with C3HS. A comparison of stress vs. control osteoblasts showed that 41 genes or ESTs displayed more than two-fold increase in expression (Table 5) whereas only 16 genes were found to be downregulated (Table 6).

Table 5. List of genes in which expression level increased more than two-fold after application of shear stress in osteoblasts isolated from B6 mice as compared to osteoblasts isolated from C3H mice. The ratios for the microarray were determined by using Genespring software.

Accession #	Fold Change	Gene Name
C81354	21.9628	
C80763	4.20637	
AF019048	3.61608	Mouse RANKL
E01057	3.34883	Mouse interleukin-1(IL-1) precursor
TC157862	3.08421	Homo sapiens mRNA; cDNA DKFZp586C1620 (from clone DKFZp586C1620); partial cds
J00370	3.03069	Mouse c-fos gene; cellular homolog to viral oncogene
AF075717	2.88893	Transforming growth factor beta 1-induced factor 2
AF053713	2.83105	Mouse Osteoprotegerin ligand
L12447	2.8031	Insuline-like growth factor binding protein 5 (IGFBP5)
TC188018	2.75545	

TC200632	2.75369	Homo sapiens CCR4-NOT transcription complex, subunit 8 (CNOT8), mRNA
AB009993	2.74642	Collagen A1(V)
X76401	2.54899	Tumor necrosis factor receptor 2
TC202099	2.51276	
D31942	2.47433	Mouse Oncostatin M
AF120489	2.45316	Growth hormone receptor/growth hormone-binding protein
X58636.1	2.41252	(LEF1) lymphoid enhancer binding factor 1
TC201479	2.39966	Homo sapiens MEBP-1 mRNA for MAPK-ERK binding protein-1, complete cds
J04069	2.39514	Insulin-like growth factor II (IGF-II)
V00727	2.38357	c-fos oncogene
AF068615	2.38111	Ciliary neutotrophic factor receptor alpha precursor
TC162168	2.37976	Homo sapiens CGI-147 protein (LOC51651), mRNA
X56848	2.3708	Bone morphogenetic protein 4 (BMP-4)
X15848	2.34551	Retinoic acid receptor gamma
U78048	2.27706	Bone morphogenetic protein type II receptor BRK-3
AJ009862	2.27282	Transforming growth factor-beta 1
L28108	2.26984	Mouse PTH/PTHrP
U51001	2.25219	DLX-1 gene
Y15800	2.23637	Mouse mRNA for G-protein coupled receptor kinase 6-D
E03515	2.21036	Mouse interleukin 6 receptor protein
SM95800	2.20214	Mouse Myogenin gene
U64331	2.18271	Mouse Osteoprotegerin (OPG)
M29464	2.17397	Mouse platelet-derived growth factor a chain (PDGA)
U36384	2.16404	Mouse twist-related bHLH protein Dermo-1
AF067191	2.14363	Fibroblast growth factor 1.a gene, exon 1
NM_010703	2.09572	Lef 1
X53802	2.07883	Mouse mRNA for interleukin-6 receptor
J05265	2.07351	Interferon gamma receptor
E04743	2.03421	Mouse IL-1 alpha
X57413	2.01756	Transforming growth factor-beta 2
SU78076	2.00177	Mouse sepiaterin reductase gene

Table 6. List of genes in which expression level decreased more than two-fold after application of shear stress in osteoblasts isolated from B6 mice as compared to osteoblasts isolated from C3H mice. The ratios for the microarray were determined by using Genespring software.

Accession #	Fold Change	Gene Name
C86942	4.135808	
C78087	2.929459	
EST03087	2.875889	
TC178738	2.715629	
C78068	2.696100	
AU022194	2.598836	
C78157	2.374702	
TC192702	2.288848	
C79008	2.271746	

AU022331	2.262090	
AU024767	2.257646	Mus musculus mRNA for PC3B protein
TC174040	2.198529	
TC163941	2.189350	
TC161597	2.065945	
TC210779	2.042810	Homo sapiens KIAA0513 gene product (KIAA0513), mRNA
C81146	2.016730	

Specific Objective 3: Validation of microarray data with Real Time PCR.

To further confirm our microarray data, we are now in the process of selecting genes for doing Real Time PCR. The selection of genes was based on: 1) confirmation of the genes known to be involved in the mechanical signaling; and 2) finding the genes or ESTs with unknown function that may be involved in the mechanical signaling. Thus, Real Time PCR was performed for a known gene (c-fos) and two ESTs (C81354 and C80763) selected from the microarray gene list. The results show that shear stress induces upregulation of c-fos and C80763 in B6 bone cells and not in C3H bone cells. These results were consistent with the data derived from the microarray analysis (Table 7). However, in case of C81354, microarray results showed a 21-fold increase in expression in B6 mice as compared to C3H mice, whereas real time PCR showed no difference in the expression level in B6 and C3H osteoblasts This shows a discrepancy between the microarray and real time PCR data and emphasizes the importance of confirming the microarray data with other, more authentic techniques as real time PCR.

Above results confirm that c-fos is involved in the mechanical signaling and further suggest that EST (accession # C80763) might play an important role in mechanical stress induced cell proliferation and differentiation which emphasizes the importance of studying this EST for its role in mechanical signaling.

Gene	**Fold Change** (Stress vs. Control)	
	Microarray	**Real Time PCR**
EST (accession# C80763	4.20	4.18
EST (accession # C81354	21.96	1.67
c-fos	3.03	2.92

Table 7. Gene expression change after fluid flow shear stress in osteoblasts isolated from B6 mice by microarray and Real Time PCR. The fold changes were defined in relative to the expression level of osteoblasts not subjected to shear stress.

Additional Progress for Technical Objective 3:

In addition to C3H and B6 mice strains, we evaluated bone formation response to loading in 6 other inbred strains of mice (129J, BALB/cByJ, NZB/BINJ, RF/J, AKR/J, and CBA/J). These additional strains of mice were selected for the following reasons: 1) to establish the mouse strain that shows the best response to loading; and 2) to select an optimal mouse pair for studies on evaluation of candidate genes involved in mediating loading response on bone. Osteoblasts isolated from these mice strains were subjected to fluid flow shear strain and thymidine incorporation was measured after 24 hours of stress. As shown in Figure 6, CBA/J, B6, RF/J, Balbc and NZB show a significant increase in the shear stress induced cell proliferation whereas C3H, 129/J and AKR showed no significant change in the shear stress induced cell proliferation as compared to the normal cells from the respective strains of mice.

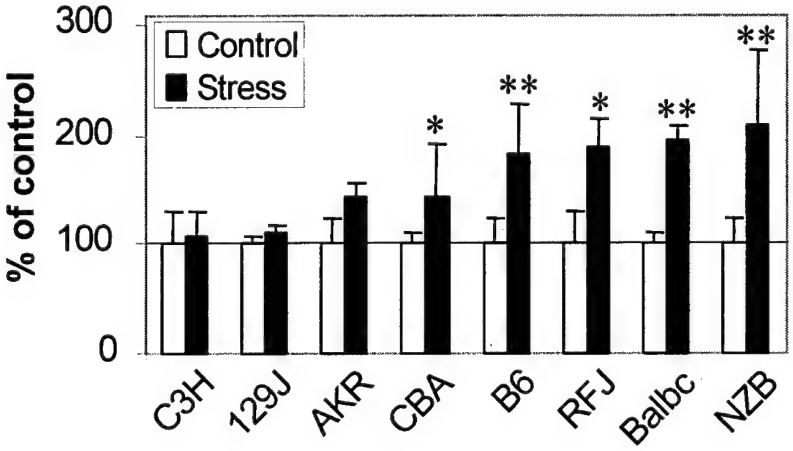

Figure 6: Effect of fluid flow shear strain on [^{3}H]thymidine incorporation in bone cells isolated from different strains of mice. Cells were subjected to fluid flow for 30 min and [^{3}H]Thymidine incorporation was measured after 24 hours of incubation. **p<0.01, *p<0.05.

Based on the response to *in vitro* mechanical loading (shear stress), the overall ranking of different mouse strains is shown in Table 8. Accordingly, C3H and 129/J seem to be poor responders whereas B6, RF/J, Balbc, and NZB seem to be good responders.

Rank	Mouse Strain	Thymidine Incorporation (% of control)	Response to Shear Stress
1	C3H	108 ± 22.69	Poor
2	129J	110 ± 08.46	Poor
3	AKR	142 ± 14.85	Medium
4	CBA	145 ± 47.06	Medium
5	B6	183 ± 46.38	Good
6	RFJ	190 ± 24.70	Good
7	Balbc	195 ± 12.93	Good
8	NZB	208 ± 70.58	Good

Table 8. Ranking of mouse strains (Good and Poor responder) based upon the thymidine incorporation in response to fluid flow shear stress in osteoblasts isolated from different mouse strains.

Reportable Outcomes

Publication:

Sonia Kapur, David J. Baylink, and K.-H. William Lau: *Fluid flow shear stress stimulates human osteoblast proliferation and differentiation through multiple interacting and competing signal transduction pathways.* Bone (2003); 32: 241-251.

Abstract:

Sonia Kapur, S.T Chen, D. J. Baylink, K.-H. W. Lau: *Extracellular Signal-Regulated Kinase (ERK)-1 and ERK2 Are Both Essential in the Mediation of The Flow Shear Strain-Induced Human Osteoblast Proliferation.* (2002); At 24th Annual Meeting of American Society for Bone and Mineral Research. San Antonio, Texas. September 20-24.

Key Findings

1. We evaluated strain-induced tyrosine phosphorylation levels of key signaling proteins in C3H and B6 mice. We studied the fluid flow induced phosphorylation of MAPK and integrin expression in these cells and found that shear strain induced a significant increase in the integrin β1expression as well as the phosphorylation levels of ERK1 and ERK2 in B6 bone cells. On the contrary, no change was observed in either integrin β1expression or phosphorylation levels of ERK1 and ERK2 in C3H bone cells in response to fluid flow.
2. We also found that the protein kinase activity of both ERK1 and ERK2 are essential for the fluid flow shear stress-induced osteoblast proliferation.
3. The most intriguing finding of this study is that overexpressing of an inactive form of ERK1 or ERK2 alone is sufficient to block the actions of endogenous ERKs in response to flow shear stress in bone cell proliferation, further suggesting that both ERK1 and ERK2 are essential for shear stress-induced proliferation of bone cells.
4. The microarray analysis revealed that with over 5,000 genes explored, 109 genes show more than a two-fold increase and 139 genes show more than two-fold decrease in expression in cells subjected to fluid flow shear stress as compared to the non-stressed cells in B6 mice. In case of C3H mice, there are 142 genes that show more than two-fold increase in expression and 135 genes that are downregulated more than two-fold in cells subjected to fluid flow shear stress as compared to the non-stressed cells. A comparison of stress vs. control osteoblasts showed that only 41 genes or ESTs displayed more than two-fold increase whereas only 16 genes or ESTs showed more than two-fold decrease in expression between B6 and C3H mice.
5. Microarray and real time PCR results confirmed that c-fos is involved in the mechanical signaling and further suggested that EST (accession # C80763) might play an important role in mechanical stress induced cell proliferation. In future studies, we shall characterize C80763 and study its role in mechanical signaling.
6. In addition to B6 and C3H, bone formation response to shear stress in six different inbred strains of mice showed that RF/J, Balbc and NZB are responsive to shear stress whereas 129/J is non-responsive to shear stress. We are now in the process of determining

whether some combination of these six strains would be more appropriate to the C3H and B6 for the high and low response pair.

Conclusions

1. The *in vitro* studies show that shear stress induces an increase in the phosphorylation levels of ERK1 and ERK2 in B6 bone cells whereas no change was seen in C3H cells. Our studies further show that the protein kinase activity of both ERK1 and ERK2 are essential for the fluid flow shear stress-induced osteoblast proliferation.
2. The microarray data reveals the list of candidate genes responsible for mediating the bone formation response to mechanical loading. With over 5,000 genes explored, 41 of these genes showed more than two-fold increase in expression in B6 bone cells above C3H cells when subjected to shear stress. These genes will now be used to further evaluate the mechanical stress differential responses between these two inbred strains of mice.
3. Based on *in vitro* studies on bone formation response to shear stress in eight different strains of mice, C3H and B6 are appropriate for the poor and good response pair to mechanical loading.

References

1. Frangos JA, McIntire LV, Eskin SG. *Shear stress induced stimulation of mammalian cell metabolism.* Biotech Bioeng (1998); 32: 1053-60.
2. Kodama Y, Uemura Y, Nagasawa S, Beamer WG, Donahue LR, Rosen CR, Baylink DJ, Farley JR. *Exercise and mechanical loading increase periosteal bone formation and whole bone strength in C57BL/6J mice but not in C3H/Hej mice.* Calcif Tissue Int (2000); 66(4): 298-306.

2. Genetic Analysis of Three Large Pedigrees with Very High Bone Density

Introduction

Quantitative traits, such as bone mineral density (BMD), are usually due to genetic contributions from multiple genes. Our long-term goal in this project is to identify those genes that contribute to peak bone density by linkage analysis studies in families with very high BMD (>2.5 SD of normal).

As reported in last year's progress report, three large pedigrees with affected members exhibiting bone density of more than 2.5 SD above the normal mean were collected. Blood was drawn from the family members in Argentina, frozen and sent to the Musculoskeletal Disease Center (MDC) for processing and analysis. At the MDC last year, genomic DNA was purified and serum marker levels of bone formation and resorption were measured. The second year of the project has focused on high-throughput genotyping for gene discovery through linkage analysis. Bone density is an important determinant of susceptibility to fracture. Thus, the identification of the genes that contribute to high bone density in these families may represent a major advance in understanding the pathways that regulate bone formation and bone healing and the pathogenesis of bone diseases such as osteoporosis.

A. Technical Objectives:

Following are the specific objectives during the second year of the grant period:

1) We will implement a whole genome screen with the ABI 377 system using multiplex PCR amplification of primer sets labeled with fluorescent labels.
2) Products will be analyzed by electrophoresis in the ABI 377 and alleles scored with appropriate software.
3) We will perform linkage analysis using the CRI-MAP, GENEHUNTER, and FASTLINK 4.0 software programs.
4) At chromosomal locations showing evidence of linkage in any of the families, additional informative markers will be genotyped to further narrow down the region of the genetic locus.

We have accomplished all of the above specific objectives. Our progress in each of the Specific Objectives is given below.

Progress on Technical Objectives

Specific Objective 1: A whole genome screen was implemented and completed for Argentina family E. 400 fluorescently labeled PCR reactions spaced at a genetic density of 10 centimorgans were amplified for all 68 individuals of the E family. Since a centimorgan corresponds to roughly one million basepairs, this corresponds to approximately one microsatellite marker every 10,000,000 basepairs to cover the entire human genome. Table 1 lists the microsatellite markers used in this study.

Genomic DNA isolated from these families is a precious resource that is difficult to obtain. Thus, our PCR reactions were optimized to use the minimal amount of genomic DNA while still amplifying robustly and uniformly. The optimal PCR reaction conditions we developed are as follows:

Reaction Mixes

9 ul of True Allele Mix (Applied Biosystems)
1 ul of Primer mix (5 uM each primer)
5 ul of genomic DNA (2 ng/ul)
Total volume = 15 ul

Thermal Cycling

Step #	Cycles	Temperature	Time
1	1	95°C	12:00
2	45	95°C	00:10
		55°C	00:15
		72°C	00:30
3	1	72°C	30:00
4	1	4°C	infinity

Table 1. Microsatellite markers used in this study and their genetic location.

Chromosome	Marker Name	Genetic Distance (centimorgans)
1	D1S468	0
1	D1S214	9.4
1	D1S450	15.9
1	D1S2667	19.9
1	D1S2697	32.9
1	D1S199	40.7
1	D1S234	50.2
1	D1S255	60.5
1	D1S2797	68
1	D1S2890	79.4
1	D1S230	90
1	D1S2841	102
1	D1S207	110
1	D1S2868	124.3
1	D1S206	133.6
1	D1S2726	142.6
1	D1S252	150.27
1	D1S498	155.89
1	D1S484	167.3
1	D1S2878	176.3
1	D1S196	181.3
1	D1S218	190.2
1	D1S238	201.1
1	D1S413	209.6
1	D1S249	219.4
1	D1S425	230.8
1	D1S213	241
1	D1S2800	250
1	D1S2785	264

1	D1S2842	273.1
1	D1S2836	284.4
2	D2S319	7.6
2	D2S2211	15.61
2	D2S162	20.03
2	D2S168	27.06
2	D2S305	38.87
2	D2S165	47.43
2	D2S367	54.96
2	D2S2259	64.29
2	D2S391	70.31
2	D2S337	80.69
2	D2S2368	85.48
2	D2S286	94.05
2	D2S2333	103.16
2	D2S2216	111.21
2	D2S160	122.96
2	D2S347	131.51
2	D2S112	141.62
2	D2S151	152.04
2	D2S142	161.26
2	D2S2330	169.41
2	D2S335	175.91
2	D2S364	186.21
2	D2S117	194.45
2	D2S325	204.53
2	D2S2382	213.49
2	D2S126	221.13
2	D2S396	232.9
2	D2S206	240.79
2	D2S338	250.54
2	D2S125	260.63
3	D3S1297	8.31
3	D3S1304	22.33
3	D3S1263	36.1
3	D3S2338	42.1
3	D3S1266	52.6
3	D3S1277	61.52
3	D3S1289	71.41
3	D3S1300	80.32
3	D3S1285	91.18
3	D3S1566	97.75
3	D3S3681	109.22
3	D3S1271	117.76
3	D3S1278	129.73
3	D3S1267	139.12
3	D3S1292	146.6
3	D3S1569	158.38
3	D3S1279	169.6

3	D3S1614	177.75
3	D3S1565	186.04
3	D3S1262	201.25
3	D3S1580	207.73
3	D3S1311	224.88
4	D4S412	4.74
4	D4S2935	13.96
4	D4S403	25.9
4	D4S419	33.42
4	D4S391	43.59
4	D4S405	56.95
4	D4S1592	69.53
4	D4S392	78.97
4	D4S2964	88.35
4	D4S1534	95.09
4	D4S414	100.75
4	D4S1572	107.95
4	D4S406	117.06
4	D4S402	124.45
4	D4S1575	132.05
4	D4S424	144.56
4	D4S413	157.99
4	D4S1597	169.42
4	D4S1539	176.19
4	D4S415	181.36
4	D4S1535	195.06
4	D4S426	206.98
5	D5S1981	1.72
5	D5S406	11.85
5	D5S630	19.67
5	D5S419	39.99
5	D5S426	51.99
5	D5S418	58.55
5	D5S407	64.67
5	D5S647	74.07
5	D5S424	81.95
5	D5S641	92.38
5	D5S428	95.4
5	D5S644	104.76
5	D5S433	111.97
5	D5S2027	119.5
5	D5S471	129.83
5	D5S2115	138.64
5	D5S436	147.49
5	D5S410	156.47
5	D5S422	164.19
5	D5S400	174.81
5	D5S408	195.49
6	D6S1574	9.18
6	D6S309	14.07

6	D6S470	18.22
6	D6S289	29.93
6	D6S422	35.66
6	D6S276	44.41
6	D6S1610	53.81
6	D6S257	79.92
6	D6S460	89.83
6	D6S462	99.01
6	D6S434	109.19
6	D6S287	121.97
6	D6S262	130
6	D6S292	136.97
6	D6S308	144.46
6	D6S441	154.1
6	D6S1581	164.78
6	D6S264	179.07
6	D6S446	189
6	D6S281	190.14
7	D7S531	5.28
7	D7S517	7.44
7	D7S513	17.74
7	D7S507	28.74
7	D7S493	34.69
7	D7S516	41.69
7	D7S484	53.5
7	D7S510	59.93
7	D7S519	69.03
7	D7S502	78.65
7	D7S669	90.42
7	D7S630	98.44
7	D7S657	104.86
7	D7S515	112.32
7	D7S486	124.08
7	D7S640	137.83
7	D7S684	147.22
7	D7S661	155.1
7	D7S636	162.33
7	D7S798	168.98
7	D7S2465	180.24
8	D8S264	0.73
8	D8S277	8.34
8	D8S550	21.33
8	D8S258	41.55
8	D8S1771	50.05
8	D8S505	60.87
8	D8S285	71
8	D8S260	79.36
8	D8S270	103.69
8	D8S1784	118.15
8	D8S514	130
8	D8S284	143.82
8	D8S272	154.02

9	D9S288	9.83
9	D9S286	18.06
9	D9S285	29.52
9	D9S157	32.24
9	D9S171	42.73
9	D9S161	51.81
9	D9S1817	59.34
9	D9S273	65.79
9	D9S175	70.33
9	D9S167	83.41
9	D9S283	94.85
9	D9S287	103.42
9	D9S1690	106.63
9	D9S1677	117.37
9	D9S1776	123.33
9	D9S1682	132.09
9	D9S290	140.86
9	D9S164	147.91
9	D9S1826	159.61
9	D9S158	161.71
10	D10S249	2.13
10	D10S591	13.49
10	D10S189	19
10	D10S547	29.15
10	D10S1653	40.36
10	D10S548	45.85
10	D10S197	52.1
10	D10S208	60.64
10	D10S196	70.23
10	D10S1652	80.77
10	D10S537	91.13
10	D10S1686	105.04
10	D10S185	116.34
10	D10S192	124.27
10	D10S597	128.73
10	D10S1693	137.39
10	D10S587	147.57
10	D10S217	157.89
10	D10S1651	168.77
10	D10S212	170.94
11	D11S4046	2.79
11	D11S1338	12.92
11	D11S902	21.47
11	D11S904	33.57
11	D11S935	45.94
11	D11S905	51.95
11	D11S4191	60.08
11	D11S987	67.48
11	D11S1314	73.64

11	D11S937	79.98
11	D11S901	85.48
11	D11S4175	91.47
11	D11S898	98.98
11	D11S908	108.59
11	D11S925	118.47
11	D11S4151	127.33
11	D11S1320	141.91
11	D11S968	147.77
12	D12S352	0
12	D12S78	11.87
12	D12S99	12.6
12	D12S336	19.68
12	D12S364	30.6
12	D12S310	36.06
12	D12S1617	44.03
12	D12S345	53.09
12	D12S85	61.34
12	D12S368	66.03
12	D12S83	75.17
12	D12S326	86.4
12	D12S351	95.56
12	D12S346	104.65
12	D12S79	125.31
12	D12S86	134.54
12	D12S324	147.17
12	D12S1659	155.94
12	D12S1723	164.63
13	D13S175	6.03
13	D13S217	17.21
13	D13S171	25.08
13	D13S218	32.9
13	D13S263	38.32
13	D13S153	45.55
13	D13S156	55.85
13	D13S170	63.9
13	D13S265	68.73
13	D13S159	79.49
13	D13S158	84.87
13	D13S173	93.52
13	D13S1265	98.82
13	D13S285	110.55
14	D14S261	6.46
14	D14S283	13.89
14	D14S275	28.01
14	D14S70	40.11
14	D14S288	47.51
14	D14S276	56.36
14	D14S63	69.18

14	D14S258	76.28
14	D14S74	87.36
14	D14S68	95.9
14	D14S280	105
14	D14S65	117.3
14	D14S985	126.61
14	D14S292	134.3
15	D15S1002	14.58
15	D15S165	20.24
15	D15S1007	25.86
15	D15S1012	35.95
15	D15S994	40.25
15	D15S978	45.62
15	D15S117	51.21
15	D15S153	62.4
15	D15S131	71.28
15	D15S205	78.92
15	D15S127	86.81
15	D15S130	100.59
15	D15S120	112.58
16	D16S423	10.36
16	D16S404	18.07
16	D16S3075	23.28
16	D16S3103	32.07
16	D16S3046	40.65
16	D16S3068	48.53
16	D16S3136	62.11
16	D16S415	67.62
16	D16S503	83.55
16	D16S515	92.1
16	D16S516	100.39
16	D16S3091	111.12
16	D16S520	125.82
17	D17S849	0.63
17	D17S831	6.6
17	D17S938	14.69
17	D17S1852	22.24
17	D17S799	31.96
17	D17S921	36.14
17	D17S1857	43.01
17	D17S798	53.41
17	D17S1868	64.16
17	D17S787	74.99
17	D17S944	82.56
17	D17S949	93.27
17	D17S785	103.53
17	D17S784	116.86
17	D17S928	126.46
18	D18S59	0

18	D18S63	8.3
18	D18S452	18.7
18	D18S464	31.17
18	D18S53	41.24
18	D18S478	52.86
18	D18S1102	62.84
18	D18S474	71.32
18	D18S64	84.8
18	D18S68	96.48
18	D18S61	105.03
18	D18S1161	114.26
18	D18S70	126
19	D19S209	10.97
19	D19S216	20.01
19	D19S884	26.37
19	D19S221	36.22
19	D19S226	42.28
19	D19S414	54.01
19	D19S220	62.03
19	D19S420	66.3
19	D19S902	72.72
19	D19S571	84.08
19	D19S418	92.56
19	D19S210	100.01
20	D20S117	2.83
20	D20S889	11.2
20	D20S115	21.15
20	D20S186	32.3
20	D20S112	39.25
20	D20S195	50.81
20	D20S107	55.74
20	D20S119	61.77
20	D20S178	66.16
20	D20S196	75.01
20	D20S100	84.78
20	D20S171	95.7
20	D20S173	98.09
21	D21S1256	9.72
21	D21S1914	19.39
21	D21S263	27.4
21	D21S1252	35.45
21	D21S266	45.87
22	D22S420	4.06
22	D22S539	14.44
22	D22S315	21.47
22	D22S280	31.3
22	D22S283	38.62
22	D22S423	46.42
22	D22S274	51.54

Following amplification, the 400 markers were pooled into 28 multiplex panels and electrophoresed with a high-density LIZ labeled size standard. Over 26,000 genotypes were generated for this family by this method. Figure 1 shows a multiplex pool of panel 28.

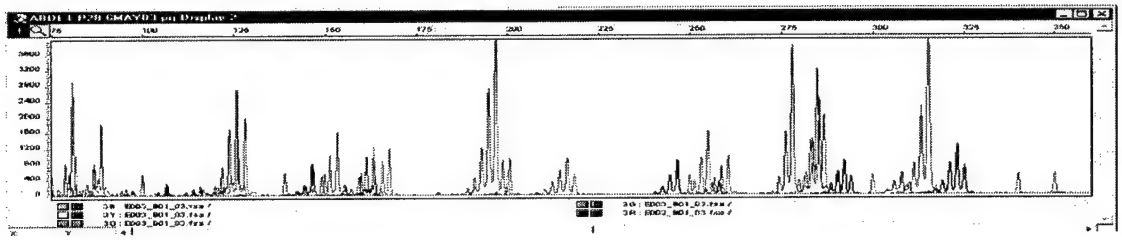

Figure 1. Multiplex pool of 18 fluorescently labeled PCR products amplified from an individual of family E. All 18 reactions were run in a single capillary on the ABI 3100 DNA analyzer. PCR reactions are labeled with FAM (blue), VIC (green), and NED (yellow, shown as black in the plot above for clarification). The labeled genotyping PCR products are co-electrophoresed with a high density size standard labeled with LIZ (orange). The x-axis is size in base pairs of the respective markers. The y-axis is fluorescent intensity.

Specific Objective 2: Following electrophoresis on the ABI 3100 DNA Analyzer, Genotyper software macros were used to semi-automatically score the allele calls for all the 28 multiplex pools of every E family individual. After initial scoring by these macros, allele calls were visually checked and edited if necessary. A table of the calls was generated and the allele sizes converted into respective allele bins. Figure 2 and Table 1 demonstrates the method used to generate all 26,000 allele calls for family E.

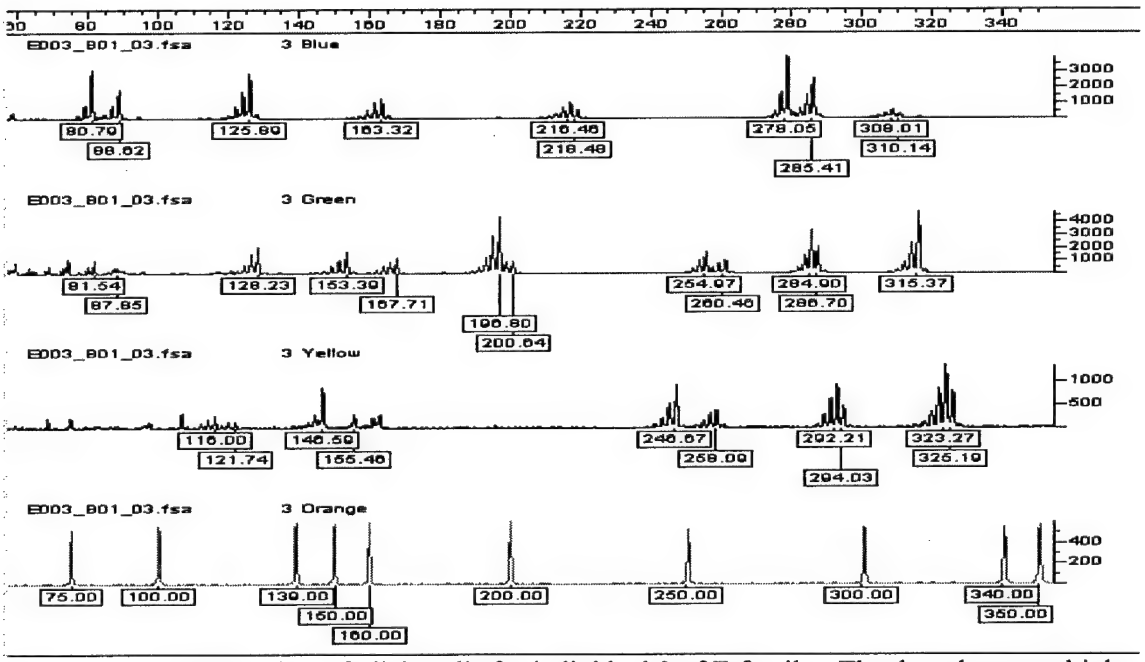

Figure 2. Genotyper plots of allele calls for individual 9 of E family. The data shows multiplex pool 28. The upper blue panel is 6 PCR reactions labeled with FAM. The center plots are 7 PCR reactions labeled with VIC (green) and 5 PCR reactions labeled with NED (yellow dye but black in plot for clarity). The lowest orange plot is the LIZ labeled molecular size standard. The macro has labeled the allele peaks with the size in nucleotide basepairs. Again the x-axis is size in nucleotides and the y-axis is fluorescent intensity.

Table 1. Genotyper macro output table of E family individual 9 for chromosome 1. The generated table lists the person ID, the capillary number the sample was run on (AbiID), the dye label color, the marker name, the multiplex panel pool, the chromosome the marker is located on, the allele sizes of the marker, the calculated allele bin numbers and whether the marker is heterozygous or homozygous for that individual.

PersID	AbiID	Dye	Marker	Panel	Chromosome	Allele1Size	Allele2Size	Allele 1 Bin Number	Allele 2 Bin Number	Heterozygosity
E009	7	G	D1S196	1	1	319.65	329.81	2	7	Het
E009	7	Y	D1S206	1	1	209.12	209.12	2	2	Homo
E009	7	Y	D1S213	1	1	116.51	118.5	8	9	Het
E009	7	B	D1S234	1	1	276.25	279.92	6	8	Het
E009	7	B	D1S249	1	1	175.7	179.49	11	13	Het
E009	7	G	D1S255	1	1	88.66	94.68	4	7	Het
E009	7	G	D1S2667	1	1	142.36	150.71	7	11	Het
E009	7	Y	D1S2726	1	1	282.54	288.16	4	7	Het
E009	7	G	D1S2785	1	1	181.01	182.95	8	9	Het
E009	7	B	D1S2797	1	1	118.82	118.82	13	13	Homo
E009	7	B	D1S2800	1	1	208.1	214.28	6	9	Het
E009	7	Y	D1S2836	1	1	247.3	251.19	4	6	Het
E009	7	Y	D1S2842	1	1	346.05	347.75	5	6	Het
E009	7	Y	D1S2878	1	1	152.75	152.75	4	4	Homo
E009	7	G	D1S2890	1	1	215.48	215.48	4	4	Homo
E009	7	B	D1S450	1	1	332.71	332.71	14	14	Homo
E009	7	G	D1S484	1	1	279.69	281.59	4	5	Het
E009	7	B	D1S199	2	1	96.21	96.21	5	5	Homo
E009	7	B	D1S199	2	1	96.02	96.02	5	5	Homo
E009	7	B	D1S207	2	1	149.91	157.97	5	9	Het
E009	7	Y	D1S214	2	1	136.25	142.54	10	13	Het
E009	7	Y	D1S214	2	1	120.63	136.23	2	10	Het
E009	7	Y	D1S218	2	1	276.5	280.28	7	9	Het
E009	7	G	D1S230	2	1	149.62	149.62	5	5	Homo
E009	7	B	D1S238	2	1	309.89	311.91	10	11	Het
E009	7	G	D1S252	2	1	87.62	87.62	3	3	Homo
E009	7	G	D1S252	2	1	87.38	87.38	3	3	Homo
E009	7	G	D1S2697	2	1	294.24	297.9	5	7	Het
E009	7	G	D1S2841	2	1	233.8	243.95	3	8	Het
E009	7	B	D1S2868	2	1	212.39	216.47	4	6	Het
E009	7	B	D1S413	2	1	253.63	257.27	4	6	Het
E009	7	Y	D1S425	2	1	346.83	346.83	4	4	Homo
E009	7	G	D1S468	2	1	206.05	208.13	10	11	Het
E009	7	Y	D1S498	2	1	200.57	200.57	9	9	Homo

Specific Objective 3: For generation of the Argentinian pedigrees, Progeny software was used. Progeny is a computer program with an integrated, customizable relational database for data management and pedigree analysis. With Progeny one can draw pedigree charts, query, sort, and import and export genetic data using it's integrated spreadsheet module. Figure 3 shows pedigree charts of the E family generated using Progeny.

Prior to linkage analysis and following generation of the allele calls and binning of the alleles, all the data was tested for potential genotyping errors and miscalls (i.e. non-hereditary due to Mendel errors) using Pedcheck software (1). Most errors found were due to incorrect binning of alleles. All miscalls and binning errors were corrected and the data tables exported as tab delimited files for linkage analysis.

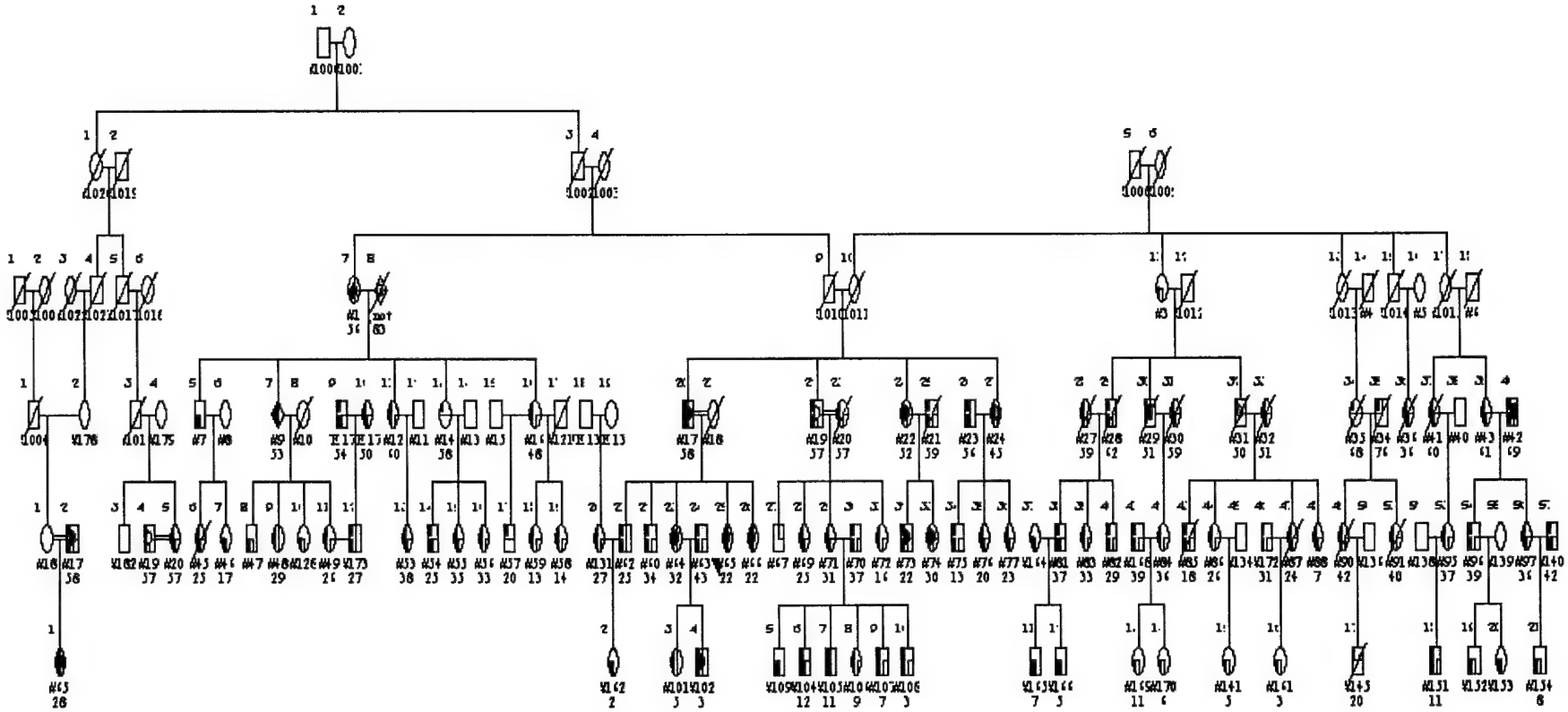

Figure 3a. Pedigree chart of the Argentina E family. The chart was generated using Progeny Software. Six generations of the E family are shown.

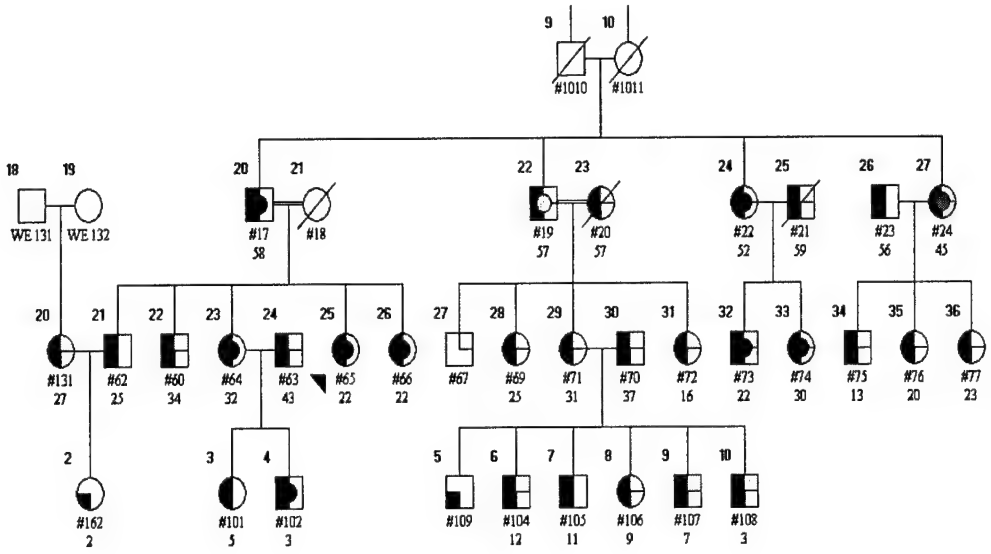

Figure 3b. Pedigree chart of smaller region of E family containing many of the individuals with high bone density. Circles indicate females and squares males. Individuals with a slash through them are deceased. The number below the circle/square indicates the coded individual identifier and beneath this the individual's age. The pedigree is color coded for sample tracking. Blue indicates that a DEXA BMD score was done on the individual, red indicates that blood was drawn and received by the MDC, yellow indicates that the individuals completed the clinical questionnaire, and center black circles indicate that the individual has very high bone density for both spine and hip (>2.5 SD above mean).

GENEHUNTER was used for linkage analysis of the genotyping data (2, 3). Several regions of the genome were found that give highly significant LOD scores. A LOD score is the logarithm of odds score, ie. the logarithm of the likelihood that two loci are linked/likelihood that loci are unlinked. Thus a LOD score of 2 indicates that there are 100:1 odds that a respective genetic region shows linkage to that trait. Figure 4 shows LOD plots for chromosomes 11 and 18 for the affected/unaffected GENEHUNTER linkage analysis of the E family. Regions of the genome that give highly significant LOD scores include parts of chromosomes 11 and 18. Additional evidence of linkage to these regions was confirmed by analyzing the data using SOLAR linkage analysis software. SOLAR stands for Sequential Oligogenic Linkage Analysis Routines, and was developed by Blangero and Almasy specifically for linkage analysis of quantitative traits in pedigrees of large size and complexity (4, 5). The CRI-MAP and FASTLINK 4.0 software programs mentioned in earlier specific objectives were developed nearly ten years ago and newer linkage analysis packages have largely superceded them.

Figure 4. LOD Score plots of GENEHUNTER linkage analysis for the E family for chromosomes 11 and 18.

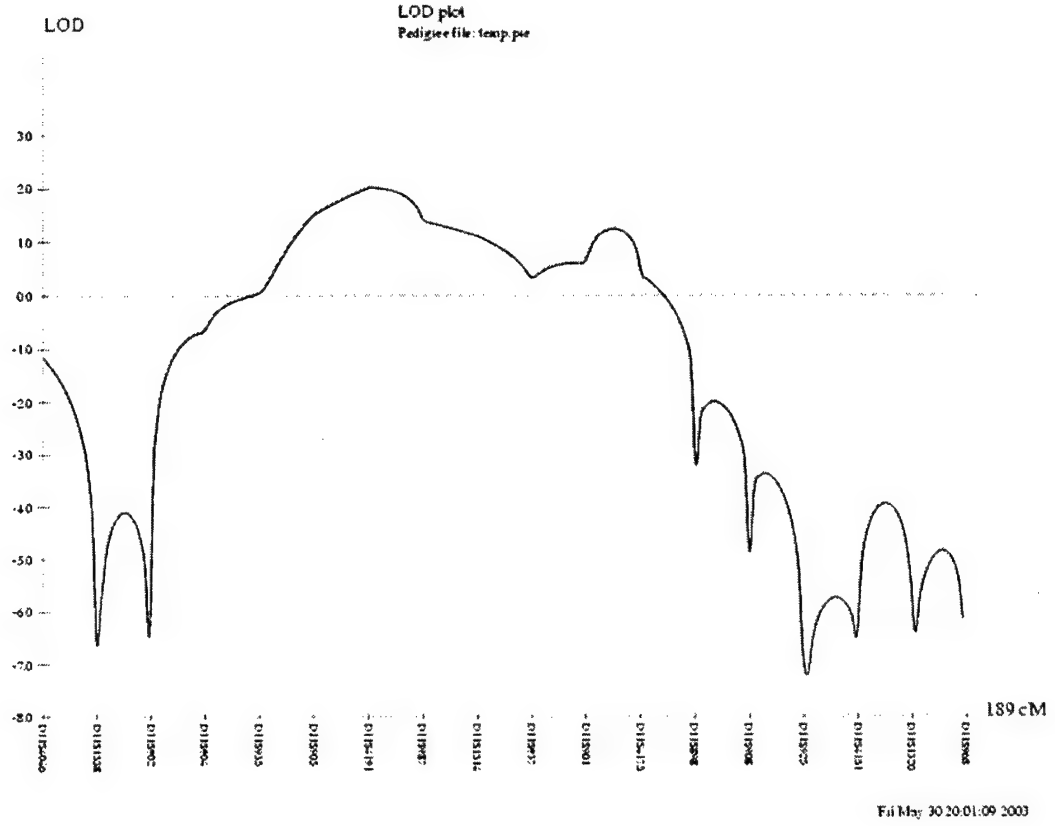

Chromosome 11 GENEHUNTER LOD Score plot. LOD scores of 2 are found at approximately 70 centimorgans form 11ptel.

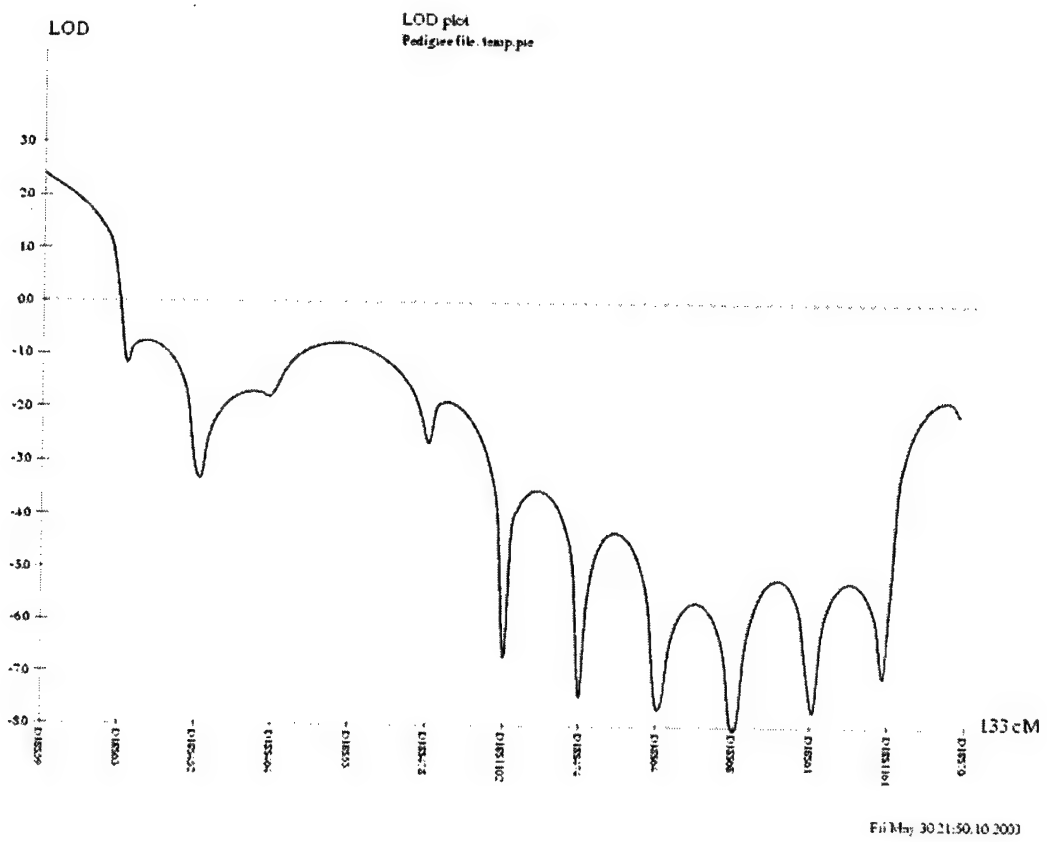

Chromosome 18 GENEHUNTER LOD Score plot. LOD scores of over 2 are found at approximately 10 centimorgans form 18ptel.

Specific Objective 4: One of the highly significant regions in the genome that gives LOD scores over 2 is a region of chromosome 11. In other studies, the LRP5 gene in this region of chromosome 11 was found to have missense mutations that contribute to high bone density (6, 7, 8). Thus in all the Argentina families we are currently in the process of screening for mutations in all exons and splice junctions of the LRP5 gene. If no mutations are found, denser targeted genotyping of chromosomes 11 and 18 will be done in the other Argentinian families. Also, we are currently examining the Celera and public genome databases to determine functional and positional candidate genes in each of the regions with significant LOD scores. This will be followed up by mutation screening of strong candidate genes and by denser more targeted genotyping of those regions to reduce the genetic distance of regions showing statistically significant genetic linkage. This will also reduce the number of candidate genes that will be needed to be screened for mutations in order to discover the gene(s) and mutation(s) contributing to high bone density.

Additional Progress

Evaluation of Biochemical Markers

To assess if the increased bone density in high bone density family members is due to increased bone formation and/or due to decreased bone resorption, we measured two bone formation markers (serum bone specific alkaline phosphatase and N-terminal Type-I procollagen peptide) and one bone resorption marker (type I collagen cross-linked N-telopeptide, NTx). All serum samples were analyzed in one batch in order to minimize the inter-assay variation. Before measurements were initiated, all assays were validated for sensitivity, intra- & inter-assay variation, interference due to hemolyzed or ecteric serum, spike recoveries, linearity and specificity. A brief description of all assays is provided below.

Alkaline phosphatase

A kinetic colorimetric assay was used to measure bone specific alkaline phosphatase (sALP). The bone specific alkaline phosphatase is determined by the heat inactivation of one aliquot of serum sample, standards and controls at 54°C for 12 minutes. The second aliquot is assayed without heating and represents the total activity. Heat inactivated normal human serum spiked with known amounts of highly purified sALP and liver alkaline phosphatase was used as standards and controls. Sensitivity of total alkaline phosphatase assay was 0.6 U/L and average intra- and inter-assay variations was CV<11%.

N-Terminal procollagen peptide (P1NP)

Serum levels of N-terminal type-I procollagen peptide were was measured by a radioimmunoassay (RIA) (manufactured by Orion Diagnostica, Finland and distributed by DiaSorin, Inc., Stillwater, MN) that utilizes a polyclonal antibody directed against the alpha 1 chain of N-terminal procollagen peptide of type-I collagen. Levels of P1NP reflect the formation of type I collagen and as such are a marker of bone formation. Results are expressed in micrograms per liter (µg/liter). The sensitivity is 2 µg/liter and average intra- and inter-assay CVs of P1NP radioimmunoassay was less than 7%.

N-Telopeptide of type-I collagen (NTx)

To assess bone resorption, we measured serum levels of type I collagen cross-linked N-telopeptides using an enzyme linked immunoassay (ELISA) (Osteomark, Ostex International. Inc., Seattle, WA, USA) that utilizes a monoclonal antibody directed against the cross-linking

domain of N-terminal peptide of type-I collagen in urine. Sensitivity of the ELISA was 5 nM BCE (bone collagen equivalent) and the linear range of the assay was 5-40 nM BCE. The average intra- and inter-assay variation for the controls was CV<9%.

Summary of Biochemical Markers Results

Bone biochemical marker levels in Family-E are shown in Table – 1. Comparison of bone biochemical markers between affected individuals in Family-E shows no differences in serum NTx and pro-collagen peptide (P1NP) levels. However, the skeletal alkaline phosphatase levels show significant differences when males and females were combined and compared with un-affected family members (Table –2). Since there were only two affected males, we did not perform any comparison between affected males and un-affected family members.

There are two types of bone diseases that can lead to high bone density: osteopetrosis and osteosclerosis. Osteopetrosis is distinguished by a low bone resorption rate, whereas osteosclerosis is distinguished by a high bone formation rate.

Our data show that for the bone resorption parameter, serum NTx was not decreased in the affected compared with the unaffected individuals pointing toward osteosclerosis and high bone formation as the cause of the high bone density. Moreover, the alkaline phosphatase was elevated in the affected individuals with the high bone density compared to the controls in the pedigree with a normal bone density. In aggregate, these data strongly suggest that the functional abnormality leading to the high bone density in this pedigree is a high bone formation rate.

Table – 1. Biochemical markers levels in Family-E

ID	Sex	Age	sNTX (nM BCE)	PINP (μg/L)	SAPL (U/L)
1	F	56	11	83.9	3.7
9	F	53	11	72.9	4.4
14	F	58	8.3	93.6	4
16	F	48	6.8	60.6	9
17	M	58	5.4	37.6	16
19	M	57	5.6	41.9	12
20	F	57	8.8	55.5	6.5
21	M	59	13	98.2	10
22	F	52	9.5	91.4	18
23	M	56	10	47.8	10
24	F	45	7.5	29.8	9.3
27	F	59	19	78.2	9.2
28	M	62	11	45.8	15
30	F	59	10	69.6	9.5
31	M	50	9.6	41.9	19
32	F	51	11	119.7	13
35	F	68	11	68.2	35

36	F	46	8.8	104.9	13
41	F	57	7.4	31.3	3.8
42	M	69	17	84.4	7.7
43	F	61	9.8	47.4	7
45	F	25	7.5	52.5	8.1
48	F	29	6.5	28.7	4.7
49	F	26	13	41.9	7.8
53	F	38	10	65.9	9.4
54	M	25	6.2	70.7	8.3
55	F	35	5.4	30.4	5.9
56	F	33	14	98.4	7.1
57	M	20	14	66.4	5.9
60	M	34	26	63.4	16
62	M	25	7	52.8	4.9
63	M	43	19	39.0	3.5
64	F	32	4.9	33.9	6.6
65	F	28	14	49.2	12
66	F	22	19	58.7	9.7
67	M		16	65.0	11
69	F	25	11	56.0	7.2
70	M	37	15	100.9	5.3
71	F	31	6.8	33.1	3.7
73	M	22	25	119.2	17
74	F	30	29	67.2	9.1
76	F	20	18	55.5	17
77	F	23	24	49.9	14
81	M	37	15	54.1	9.7
82	M	29	25	70.2	11
83	F	33	17	55.7	6
84	F	36	10	21.2	3.4
85	M	18	29*	163.9*	37*
86	F	26	49*	234.8*	50*
87	F	24	74*	631.9*	51*
90	F	42	19	40.3	9
91	F	40	18	19.4	5.3
95	F	37	36*	36.8	7.4
96	M	39	11	66.9	13
97	F	36	7.3	75.7	5.4
131	F	27	23	47.4	3.5
140	M	42	27	73.5	8.8
145	M	20	88*	285.8*	51*
164	F	34	11	32.2	3.8
168	M	39	23	72.8	15
172	M	31	18	34.3	3.7
173	M	27	10	60.1	7.9
WE 173	M	54	13	29.0	9.2
WE 174	F	50	8.1	61.7	19

*Due to very high values (higher than clinical reportable range for these analytes) in these patients, we excluded these samples from our analysis.

Table – 2. Comparison of skeletal alkaline phosphatase between affected individuals and normal family members

Study Groups	n	Age (Mean ± SD)	sALP (Mean ± SD)	Difference	p-Value (Mann-Whitney TTest)
*Affected Male+Female	7	34.9 ±14.4	12.6 ±4.4	46%	0.0299
Normal Male+Female Family Members	50	41.1±12.8	8.6 ±4.3		
Affected Female	5	32.8±11.4	11.1 ±4.4	38%	0.0914
Normal Female Family Members	31	41.3±12.5	8.0 ±4.3		

*Marker levels are affected by both age and sex and hence these factors should be taken into account before any comparison. However, because of only few affected members and limited number of age and sex matched family members, we have performed analysis of males and females combined together as well as separately.

Key Findings

1. We completed a whole genome screen at a density of 10 centimorgans. This screen involved generating over 26,000 genotypes for all individuals in the Argentina E family.

2. PCR methods and fluorescent multiplexing pools were developed and optimized to minimize the amount of genomic DNA needed to generate a whole genome screen. The amount of genomic DNA we now need for a 10-cM genome screen is approximately 5 micrograms vs. 25 micrograms in standard protocols. This conserves the rare DNA samples that took several years to collect and isolate.

3. Genotyping macros were developed to semi-automatically call and generate data tables for all 26,000 genotypes.

4. PedCheck software was installed and utilized to insure that the data generated was high quality with no Mendel errors and suitable for linkage analysis.

5. GENEHUNTER and SOLAR linkage analysis was implemented and completed with the E family data.

6. Regions of highly statistically significant (>2 LOD scores) were found on chromosomes 11 and 18.

7. Public and private databases of the genomic regions of significant linkage are being searched for positional and functional candidate genes.

8. Additional mutational screening of strong candidate genes is being undertaken as well as denser more focused genotyping in those statistically significant genomic regions.

9. All serum biochemical marker assays have been completed. From the serum data, we make the following findings:
    a) The higher sALP values in affected member are consistent with the prediction that increased bone formation may contribute to higher bone mineral density in these patients.
    b) Since NTx values are not decreased in patients with high bone mineral density, the decreased bone turnover is less likely an explanation for the higher bone mineral density.

Reportable Outcomes
None yet.

Conclusions

There is strong evidence that we have located a site on chromosome 11 that is responsible for the high bone density phenotype in the Argentina E family. This is under further investigation through additional fine genetic mapping and by mutational screening of candidate genes. We have found additional evidence that chromosome 18 may harbor a modifying locus in this family. Additional experiments will be undertaken to confirm these results and discover the gene(s) and mutation(s) involved in the high bone density phenotype.

References:

1. O'Connell JR and Weeks DE. "PedCheck: A Program for Identification of Genotype Incompatibilities in Linkage Analysis." *Am J Hum Genet* 63:259-266 (1998).

2. Kruglyak L, Daly M, Reeve-Daly M, and Lander E. "Parametric and Nonparametric Linkage Analysis: A Unified Multipoint Approach." *Am J Hum Genet* 58: 1347-1363 (1996).

3. Pratt SC, Daly MJ, Kruglyak L. "Exact Multipoint Quantitative-Trait Linkage Analysis in Pedigrees by Variance Components." *Am J Hum Genet* 66(3):1153-7 (2000).

4. Almasy L and Blangero J. Multipoint quantitative trait linkage analysis in general pedigrees. *Am J Hum Genet* 62:1198-1211 (1998).

5. Blangero J and Almasy L. Multipoint oligogenic linkage analysis of quantitative traits. *Genet Epidemiol* 14:959-964 (1997).

6. Boyden,L.M., Mao,J., Belsky,J., Mitzner,L., Farhi,A., Mitnick,M.A., Wu,D., Insogna,K. and Lifton,R.P. "High Bone Density due to a Mutation in LDL-Receptor-Related Protein 5." *N. Engl. J. Med.* 346 (20), 1513-1521 (2002).

7. Little,R.D., Carulli,J.P., Del Mastro,R.G., Dupuis,J., Osborne,M., Folz,C., Manning,S.P., Swain,P.M., Zhao,S.C., Eustace,B., Lappe,M.M., Spitzer,L., Zweier,S., Braunschweiger,K., Benchekroun,Y., Hu,X., Adair,R., Chee,L., FitzGerald,M.G., Tulig,C., Caruso,A., Tzellas,N., Bawa,A., Franklin,B., McGuire,S., Nogues,X., Gong,G., Allen,K.M., Anisowicz,A., Morales,A.J., Lomedico,P.T., Recker,S.M., Van Eerdewegh,P., Recker,R.R. and Johnson,M.L. "A Mutation in the LDL Receptor-Related Protein 5 gene Results in the Autosomal Dominant High-Bone-Mass trait." *Am. J. Hum. Genet.* 70 (1), 11-19 (2002).

8. Gong,Y., Vikkula,M., Boon,L., Liu,J., Beighton,P., Ramesar,R., Peltonen,L., Somer,H., Hirose,T., Dallapiccola,B., De Paepe,A., Swoboda,W., Zabel,B., Superti-Furga,A., Steinmann,B., Brunner,H.G., Jans,A., Boles,R.G., Adkins,W., van den Boogaard,M.J., Olsen,B.R. and Warman,M.L. "Osteoporosis-Pseudoglioma Syndrome, a Disorder Affecting Skeletal Strength and Vision, is Assigned to Chromosome Region 11q12-13." *Am. J. Hum. Genet.* 59 (1), 146-151 (1996).